Alma Mater Studiorum – Università di Bologna

DOTTORATO DI RICERCA IN

INGEGNERIA BIOMEDICA, ELETTRICA E DEI SISTEMI

Ciclo XXXI

Settore Concorsuale: 09 / G1 - AUTOMATICA

Settore Scientifico Disciplinare: ING-INF / 04 - AUTOMATICA

Haptic Control of Mobile Manipulators Interacting with the Environment

Presentata da: Davide Chiaravalli

Coordinatore Dottorato **Supervisore**

Prof. Daniele Vigo **Prof. Claudio Melchiorri**

Esame finale anno 2019

ALMA MATER STUDIORUM, UNIVERSITY OF BOLOGNA

Abstract

School of Engineering and Architecture
Department of Electrical, Electronic and Information Engineering (DEI)

Doctor of Philosophy

Haptic control of mobile manipulators interacting with the environment

by Davide CHIARAVALLI

In the modern society the haptic control of robotic manipulators plays a central role in many industrial fields because of the improvement of human capabilities and the prevention of many hazards that it can provide. Many different studies are focusing on the improvement of the operator experience, aiming at simplifying the control interface and increasing the level of intuitiveness that the system can provide to a non-trained user. This work focus on the control of mobile manipulator platforms, that are gaining popularity in the industrial world because of their capability to merge the manipulation of the environment with a potentially infinite workspace. In particular three different aspects concerning the haptic shared control of mobile manipulators will be studied. Initially the manipulation of liquid container is analyzed and a new feed-forward filtering technique able to guarantee a slosh free motion without any a priori knowledge of the imposed trajectory is proposed. Then the trajectory planning for a mobile base in an unstructured environment is considered. A new planner based on the properties of B-spline curves is studied and tested for both the haptic and the autonomous case. Eventually the control of a mobile manipulator by means of a single commercial haptic device is addressed. A new mapping technique able to provide an intuitive interface for the control for the human operator is presented. The effectiveness of the proposed works is confirmed via several experimental tests.

Contents

List of Figures

List of Tables

List of Symbols

b	offset	
b_{visc}	damping factor	
d	distance	m
e	effort	
E	energy	J
f	flow	
F	force vector	N
F_{el}	elastic force	N
F_m	force exerted on the master side	N
F_s	force exerted on the slave side	N
F_v	viscous force	N
h	liquid heigth	m
k	scale factor	
k_{bal}	ballistic control scale factor	
k_{drift}	drifting control scale factor	
k_{el}	elastic spring stiffness	
k_p	k_bal incremental factor	
k_r	ballistic control incremental factor	
k_{rp}	positive value of k_r	
k_{rn}	negative value of k_r	
k_{rate}	rate control scale factor	
k_v	virtual mass control factor	
K	kinetic energy	
l	length	m
L	distance from nearest obstacle	
m	mass	kg
p	trajectory via point	m
P	power	W
r	radius	m
R	radius of spherical region	m
R_i	radius of the grasping area	m
R_m	radius of the master workspace	m
R_o	external radius of the transition area	m
t	time	s
t_k	time knot	s
T	period	s
v	velocity of the mobile base	$\mathrm{m\,s^{-1}}$
v_h	velocity threshold	$\mathrm{m\,s^{-1}}$
x	position coordinate along the x axis	m
x_c	position of the container along x	m

x_m	position of the pendulum mass along z	m
$\dot{x}$	velocity along the x axis	$\mathrm{m\,s^{-1}}$
$\dot{x}_c$	velocity of the container along x	$\mathrm{m\,s^{-1}}$
$\dot{x}_m$	velocity of the pendulum mass along x	$\mathrm{m\,s^{-1}}$
$\dot{x}_v$	velocity of the mobile base along x	$\mathrm{m\,s^{-1}}$
$\ddot{x}_c$	acceleration of the container along x	$\mathrm{m\,s^{-2}}$
X	position vector	m
X_m	position of the master	m
X_s	position of the slave	m
X_ω	position of the master reference frame	m
$\dot{X}$	velocity vector	$\mathrm{m\,s^{-1}}$
$\dot{X}_m$	velocity of the master	$\mathrm{m\,s^{-1}}$
$\dot{X}_s$	velocity of the slave	$\mathrm{m\,s^{-1}}$
$\dot{X}_v$	velocity of the virtual mass	$\mathrm{m\,s^{-1}}$
$\dot{X}_\omega$	velocity of the haptic reference frame	$\mathrm{m\,s^{-1}}$
y	position coordinate along the y axis	m
$\dot{y}_v$	velocity of the mobile base along y	$\mathrm{m\,s^{-1}}$
z	position coordinate along the z axis	m
z_c	position of the container along z	m
z_m	position of the pendulum mass along z	m
$\dot{z}_c$	velocity of container along z	$\mathrm{m\,s^{-1}}$
$\dot{z}_m$	velocity of pendulum mass along z	$\mathrm{m\,s^{-1}}$
$\dot{z}_v$	velocity of the mobile base along z	$\mathrm{m\,s^{-1}}$
$\ddot{z}_c$	acceleration of the container along z	$\mathrm{m\,s^{-2}}$
Z	impedance	$\mathrm{N\,s\,m^{-1}}$
Z_0	impedance of the transmission line	$\mathrm{N\,s\,m^{-1}}$
Z_{in}	impedance felt at the master	$\mathrm{N\,s\,m^{-1}}$
Z_{out}	impedance felt by the slave	$\mathrm{N\,s\,m^{-1}}$
β	tilting angle	rad
δ	damping factor	
ω	angular velocity	$\mathrm{rad\,s^{-1}}$
ω_n	natural fraquency	rad
ω_L	angular velocity of the left wheel	$\mathrm{rad\,s^{-1}}$
ω_R	angular velocity of the right wheel	$\mathrm{rad\,s^{-1}}$
θ	angular position	rad
Φ	potential	J

Dedicated to my family

Introduction

The concept of "Robot", a mechanical system able to perform predefined tasks aimed at simplifying the life of the human society, was well known centuries before its definition in 1920. Since the early ages of humanity, mechanical machines have been built with the purpose to assist and simplify many jobs carried out by human workers. Particular attention was provided to the extension of human capabilities and to the reduction of labour force required to complete a given assignment within a certain time window. Despite the huge number of different applications and fields in which robotic machines have been built, the final purpose has always been the interaction and manipulation of the considered environment. Nowadays the third industrial revolution has drawn more complex scenarios: a robotic system is not just mechanical any more but it is instead characterized by different components and subsystems related to several disciplines among which electronic, optimization, informatics and computer vision. The actual robot is a system capable of gaining feedbacks of different type and is required to achieve a flexible and reactive interaction with the environment according to its actual state. Given its capabilities new problems have arisen in this research field, considering applications that do not address only human work, but also everyday life situations. The research is then now focusing on improving the flexibility of the systems and increasing their ability to assist and interact also with other human beings.
In this scenario the haptic control, i.e. the control of a robotic system from a distance, covers an important role. Several applications as a matter of fact still do require the presence of the human operator in the control loop , where sometimes he takes the role of the supervisor or, in some specific cases, of the direct actor:

- In applications where the environment could be dangerous the operator can safely manipulate from the distance (e.g. radioactive material handling) or can supervise the behaviour and movements of the system (e.g planet exploration)
- In applications based on learning by doing, where complex reactions have to be extrapolated from the manipulator, the user can command and show the system how to perform different assignment so that the system can learn to replicate and extend them.
- In applications where the task has still too many variables to handle, the human being still works as a "safety" system (autonomous car control).

This work focuses on the haptic control of a specific type of robotic systems: the mobile manipulators. A mobile manipulator is characterized by a mobile base and one or more robotic arms. This kind of platform merges together the dexterity of the arms and the mobility of the base, allowing to increase indefinitely the dimension of the manipulation workspace of the robot. Because of their flexibility and improved capabilities this kind of platforms are currently researched in many different fields, in particular in studies concerning the interaction and collaboration with humans

in unstructured environments. This thesis deals with the analysis and study of different aspects that concern the haptic manipulation carried out in unstructured and close environment, with particular attention to the simplification of the control task for the human operator. In particular three main aspects will be considered:

- The manipulation of an object, in particular a liquid-filled vessel, while at the same time suppressing the sloshing of the liquid
- The definition of the trajectory to follow for both the arm and the base in presence of obstacles and humans.
- The characterization of the haptic control and mapping for the robot

Despite these aspects being addressed separately, their purpose as components embedded in a control interface for a simplified control of a mobile manipulator in an unstructured and complex environment will be discussed and analyzed. The proposed work is divided in five chapters.
In Chapter 1 a generic haptic system will be presented and modelled. Several key problems as the control in presence of time delays and the mapping strategies for the haptic system will be presented and addressed. The state of the art algorithm addressing these problems will be also introduced. In Chapter 2 a plug-in feedforward filter to prevent sloshing in haptic liquid handling is proposed. The liquid is modelled as a fixed mass and a series of inverse pendulums. The vibrations and the sloshing are suppressed by the application of a damped harmonic smoother and a proper reorientation of the vessel. The experimental tests shows the effectiveness of the proposed approach.
Chapter 3 will address the definition of the commanded trajectories for the haptic system considering an unstructured environment. A simple and effective planner exploiting the properties of uniform B-splines is studied and evaluated. Various tests are performed under different environment condition and modelling.
In Chapter 4 the mapping problem for the control of a mobile manipulator will be addressed. Current methods involve the definition of two separate control algorithm for the mobile base and the robotic arm. A new mapping technique aimed at using a single haptic device for the control and at abstracting the operator from the two low level control structures is presented. Several tests performed with different robotic platforms and different users will confirm the capabilities of the new algorithm.
Eventually Chapter 5 will propose some considerations on this work and the future directions of research.

Chapter 1

The haptic control

1.1 Robotic teleoperation

The teleoperation, or the ability to control robotic platforms at distance, is a field of robotics that has become quite important because of the possibility to increase human capabilities way beyond their normal limits. Since the first studies in 1940's the research field has been contributed with a huge number of works that have led to continuously increased performance and improved control structures [1] [2] [3] [4]. A teleoperation system is characterized by five main components:

- **The human operator**: the person that is controlling the system and interacting with it to command a desired behaviour;
- **The master device**: the robotic platform (named haptic device) through which the operator sends signals to the system;
- **The slave device**: the robotic platform that is commanded by the operator motion through the master device;
- **The communication channel**: the physical channel used to carry all the informations between the two robotic devices;
- **The environment**: the partially unknown and responsive system the slave device interacts with.

This control structure has been exploited in many different application fields because of the possibility to improve human perception and strenght and also to separate the human operator from the workspace of the slave, preventing many possible hazards that could be caused by dangerous environments. This becomes particularly interesting in operations that concern the handling of poisonous or toxic material or motion in human-unfriendly environments like in space travel or underground exploration. It also proves crucial in surgery operations, where the enhanced sensitivity that the teleoperation could provide improves the capabilities of the surgeon. According to the different type of task requested, several control paradigm have been developed.

A generic teleoperation system can be modelled according to a 2-port representation, see Fig. 1.1 [5] [6] [7] [8]. In order to understand the model some concept on port modelling theory are provided. Port modelling of dynamical systems is a field of research that studies the power exchange between interconnected systems. A port is an interconnection between two or more subsystems where power can be

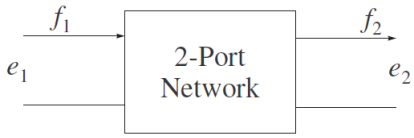

FIGURE 1.1: 2-port representation of a generic system.

exchanged. The power in any physical system is characterized by the product of two variables defined as effort and flow:

$$P(t) = e(t)f(t). \tag{1.1}$$

In a teleoperation system usually the velocity imposed on the slave is considered the flow variable while the force feedback induced on the operator is the effort variable. Their product defines the total power exchanged with the slave subsystem. The behaviour of the network can be described using different matrix representations according to the chosen input variable. If both the master and the slave side are controlled in velocity the system can be described by an impedance relation:

$$\begin{pmatrix} F_m \\ F_s \end{pmatrix} = \begin{pmatrix} z_{11} & z_{12} \\ z_{21} & z_{22} \end{pmatrix} \begin{pmatrix} \dot{X}_m \\ \dot{X}_s \end{pmatrix} \tag{1.2}$$

Where F_m and F_s are the effort variables at the two sides (force exerted) and $\dot{X}_m$ and $\dot{X}_s$ are the flow variables (velocities of the subsystems). A more common modelling considers the force available on slave side and leads to an hybrid model:

$$\begin{pmatrix} F_m \\ -\dot{X}_s \end{pmatrix} = \begin{pmatrix} h_{11} & h_{12} \\ h_{21} & h_{22} \end{pmatrix} \begin{pmatrix} \dot{X}_m \\ \dot{F}_s \end{pmatrix} = H(s) \begin{pmatrix} \dot{X}_m \\ \dot{F}_s \end{pmatrix} \tag{1.3}$$

The hybrid matrix elements can be interpreted as follows:

$$H(s) = \begin{pmatrix} Z_{in} & ForceScaling \\ VelocityScaling & -Z_{out}^{-1} \end{pmatrix} \tag{1.4}$$

The ideal teleoperation network, providing the concept of full transparency first proposed by Lawrence[9], would provide to the operator the same values of force and velocity at the slave side, having:

$$H(s) = \begin{pmatrix} 0 & 1 \\ -1 & 0 \end{pmatrix} \tag{1.5}$$

This has been proved to be not feasible, therefore some level of trade-off must be considered, especially in presence of time delays. In particular to improve transparency both effort and flow signal should be transmitted through the network[9]. The new architecture obtained consider a 4-channel control as shown in Fig. 1.2. As can be seen in the picture, the system is characterized by six independent control block that should be optimized in order to maximize transparency.

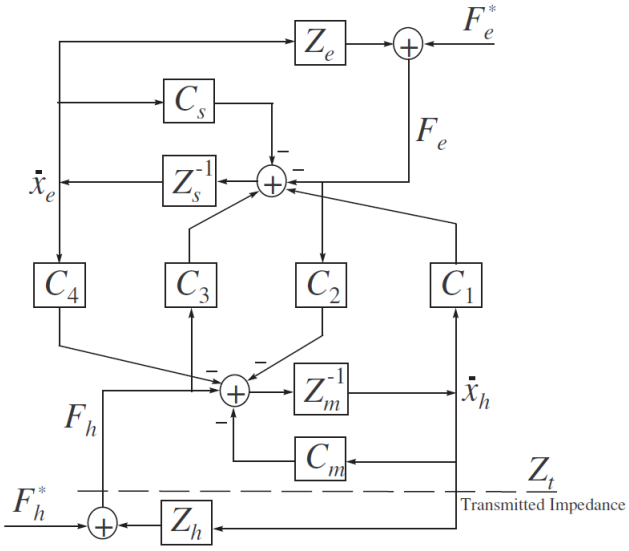

FIGURE 1.2: 4 channel representation of a generic teleoperation system.

From the control perspective all teleoperation algorithms focus on three main aspects:

- **Stability**: the overall control system must be kept stable regardless of the presence of time delays or any action induced by the operator or the environment;
- **Telepresence**: the system should provide by means of different feedbacks to the operator the feeling of being immersed in the slave device environment;
- **Transparency**: the system should make the operator feel the same interaction the slave robot is experiencing with the environment [9].

Since the master and the slave device can be placed at great distance from each other a major role in the system is played by the control layer that manages the exchange of information along the communication channel. In these situations the handling of time delays in the network becomes crucial. The most common techniques to handle time delays involve the use of the scattering approach or wave variables and are based on passivity theory. The scattering approach [10] is based on the scattering operator, defined in terms of an incident wave $f(t) + v(t)$ and a reflected wave $f(t) - v(t)$ as follows:

$$F(t) - \dot{X}(t) = S(F(t) + \dot{X}(t)) \tag{1.6}$$

where the scattering operator is defined as

$$S(s) = \begin{pmatrix} 1 & 0 \\ 0 & -1 \end{pmatrix} (H(s) - I)(H(s) + I)^{-1} \tag{1.7}$$

In order to guarantee passivity the energy content of the incident wave must be greater than the one of the reflected wave. Therefore the teleoperation system is

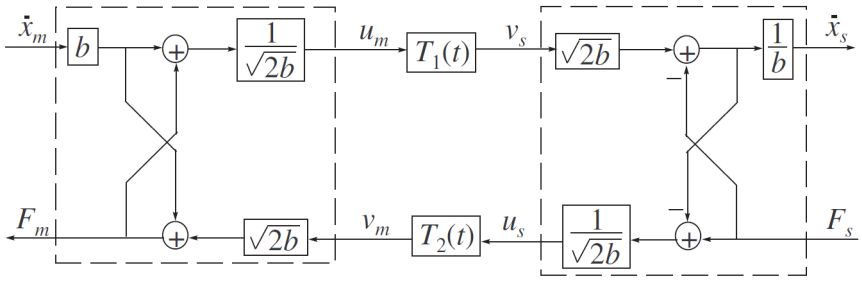

FIGURE 1.3: modelling of the communication network in a wave variable framework.

passive if the infinity norm of the scattering operator $\|S\|_\infty$ is less than 1. This way the transmission model that makes the channel passive becomes:

$$F_m(t) = F_s(t-T) + Z_0(\dot{X}_m(t) - \dot{X}_s(t-T)) \tag{1.8}$$

$$\dot{X}_s(t) = \dot{X}_m(t-T) + Z_0^{-1}(F_m(t-T) - F_s(t)) \tag{1.9}$$

The same result is obtained using the wave variable formulation [11]. Wave variables are defined as:

$$u_m = \frac{1}{\sqrt{2b}}(F_m(t) + Z_b\dot{X}_m(t)) \tag{1.10}$$

$$u_s = \frac{1}{\sqrt{2b}}(F_s(t) - Z_b\dot{X}_s(t)) \tag{1.11}$$

where b is the characteristic impedance of the transmission line modelled as shown in Fig. 1.3. In presence of constant time delays the energy of the transmission system is defined as:

$$E(t) = \frac{1}{2}\int_{t-T}^{t}(u_m^T(\tau)u_m(\tau) + u_s^T(\tau)u_s(\tau))d\tau > 0 \tag{1.12}$$

that proves the passivity of the channel. Many different studies and passivity based approaches [12] [13] [14] have been developed in the last decades guaranteeing very high level of optimization in the trade off between transparency and complexity of the system [15] [16]. Despite many researchers still working actively on these topics, recent studies are being focusing on different aspects of the teleoperation system. A recent research has in fact showed how the transparency in the system affects the user experience and performance only up to a certain degree, after which the performance-transparency curve saturates[17]. This has led to different studies focused on the experience of the operator, on how to improve its performance, reduce the complexity of its tasks and the expertise required to carry them to the end. A new deal of attention has then been directed toward control schemes that could focus on performance instead of transparency. This has led to the development of hybrid schemes where some intelligence was provided to the controlled system, that was able to cooperate together with the operator for the accomplishment of the task.

In light of this new characterization the teleoperation algorithms can be grouped in 4 different families:

- **Closed loop control**(direct teleoperation): the operator directly controls the actuators of the slave system (possible only with minimum delays)
- **Coordinated control**: the operator controls the actuators but some internal control loop regulates low level controls, especially in presence of time delays
- **Supervisory control**: the system is gained an high degree of autonomy and the operator acts as a supervisor, just giving high level control signals
- **Shared control**: the system cooperate together with the operator, providing some autonomous motion and custom made feedback to simplify the operator task.

Shared control is showing promising results in term of increasing performance once a good transparency trade-off has been obtained.[17]

1.2 Master-slave workspace mapping

One of the main problems in the definition of a teleoperation system is the development of the mapping algorithm between the master and the slave workspace. Usually in fact haptic device are characterized by small workspaces that would allow the operator to control the system with minimal effort. On the other hand such small dimension could become a problem when the controlled manipulator spans a much larger space. In this scenario the definition of a valid mapping for the system proves crucial. Let's consider the mapping for the control of the end effector position X_s of a robotic manipulator in the operational workspace. On the master side the haptic device has its cursor at the position X_m with respect to the haptic reference frame, that is posed in a predefined point X_w with respect to the global reference frame. Among all the mapping techniques three main strategies can be deduced [18]:

- **Position control**: The workspace of the slave is directly mapped in that of the master. A displacement of the master pose directly induce a proportional displacement of the slave, scaled by an appropriate factor k. When the haptic device is not moving also the slave device can not change position.

$$X_s = k_p X_m + X_w \tag{1.13}$$

- **Rate control**: The dynamic of the slave motion is controlled by the position of the master. This scheme is characterized by a misplacement between the movements of the two systems, so that motion of the slave is allowed even when the master is not moving.

$$\dot{X}_s = k_{rate}(X_m - X_w) \tag{1.14}$$

- **Ballistic control**: The relative position between the reference frames of the slave and the master devices is not constant in time. This control strategy is used to address the reduction in resolution caused by a big mismatch in workspace dimensions. The scaling factor is modified according to the master

velocity. This way is possible to obtain both a fine motion control when the operator works with slow movement to gain resolution and a course control when fast motions along the workspace are required:

$$\dot{X}_s = k_{bal}(\dot{X}_m, t)\dot{X}_m \tag{1.15}$$

kbal is the dynamic scale factor changing in time according to

$$k_{bal} = k_r t + k_{bal_0} \tag{1.16}$$

where k_{bal_0} is the scale factor initial value and k_r is an incremental factor given by:

$$k_r = \begin{cases} k_{rp}\|\dot{X}_m\| & \text{if } \|\dot{X}_m\| > v_h \\ k_{rn} & \text{if } \|\dot{X}_m\| < v_h. \end{cases} \tag{1.17}$$

k_{sp} and k_{sn} represent the positive and negative incremental factor respectively while v_h defines the velocity threshold for the switch between the two modes.

In addition several hybrid techniques that try to put together the advantages provided by the different techniques have been studied. Different techniques have been developed according to the required characteristics of the slave device.

1.2.1 Robotic manipulator mapping

Robotic manipulator are characterized by a finite dimension workspace that usually spans a much larger space than the haptic device. Since robotic arms are usually involved in manipulation tasks the trade-off between the working precision and the simplicity of motion in the whole workspace becomes a central issue. In order to address this problem more complex techniques have been developed taking into consideration hybrid approach with respect to the standard ones.

Drifting control [19] [18] is a method to impose additional motion to the haptic frame with the purpose of simplify the task of moving inside a larger workspace. In this case the haptic frame is not fixed and slowly drifts toward the haptic reference position, with a velocity value low enough not to be perceptible by the human user. This way the operator itself is unconsciously driven to correct the drift and is kept away from the workspace boundaries while at the same time mantaining a high work resolution. The haptic reference moves according to:

$$\dot{X}_w = \frac{k_{drift}}{R_m}|\dot{X}_h|(X_h - X_w) \tag{1.18}$$

where k is the drift factor and R_m is the radius of the smallest sphere that encloses the device workspace. Once the drift of the reference frame is evaluated the final velocity of the arm is obtained through equation (1.13).

Modified rate control [20] [21] is another technique to increase the precision of the manipulation while keeping a simplified motion around all the workspace. The control strategy is divided in two different modes:

- in the first mode the system uses a standard position mapping (see (1.13)) with a scale factor that guarantees an high enough precision;

- in the second mode, usually enabled by a physical switch, the reference frame position of the master device with respect to the slave one is moved along the imposed direction:

$$X_w = X_w + \dot{X}_h \frac{(X_h - X_w)}{\|(X_h - X_w)\|} \tag{1.19}$$

Bubble control is an hybrid control scheme that tries to put together the advantages of both position and rate control strategies. The workspace of the master device is divided in two concentrical regions. In the inner region a standard position control is applied see (1.13), while in the outer region a velocity rate control is chosen, see (1.14). This way the arm can be controlled with fine control in a small region and eventually driven to others when the considered portion of the workspace in no longer of interest.

1.2.2 Mobile base mapping

The teleoperation control of a mobile base is characterized by an infinite dimension workspace. In addition some non-holonomic constraints are present in most of the modern robotic structures. This situation has determined the focus on rate control algorithms, able to handle large workspaces with the disadvantage of a lower precision in positioning, usually less important for mobile platforms.
Let's consider a unicycle mobile platform. Its kinematic model is expressed by:

$$\begin{pmatrix} \dot{x}_v \\ \dot{y}_v \\ \dot{\theta}_v \end{pmatrix} = \begin{pmatrix} \cos\theta_v & 0 \\ \sin\theta_v & 0 \\ 0 & 1 \end{pmatrix} \begin{pmatrix} v(t) \\ \omega(t) \end{pmatrix} \tag{1.20}$$

where (x_v, y_v, θ_v) represent the vehicle pose in the global reference frame and $(v(t), \omega(t))$ the linear and angular velocity respectively of the mobile base with respect to its reference frame. In order to address all possible movements in space a differential drive model is considered, see figure Fig. 1.4.

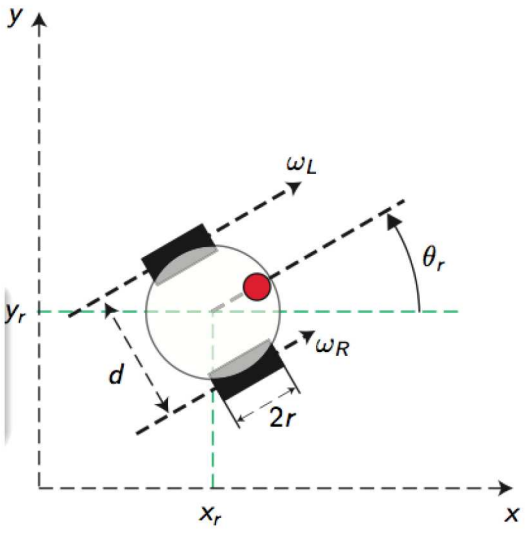

FIGURE 1.4: unicycle differential drive.

Let's consider ω_L, ω_R the velocities of the two wheels, the wheels radius r and the distance between the wheels d. The motion law of the wheels can be mapped in the motion of the robot in the plane by:

$$\begin{pmatrix} v(t) \\ \omega(t) \end{pmatrix} = \begin{pmatrix} \frac{r}{2} & \frac{r}{2} \\ \frac{r}{d} & \frac{r}{d} \end{pmatrix} \begin{pmatrix} \omega_L(t) \\ \omega_R(t) \end{pmatrix} \tag{1.21}$$

This way by joining (1.20) and (1.21) the final movement of the robot with respect of the wheel can be obtained:

$$\begin{pmatrix} \dot{x}_v \\ \dot{y}_v \\ \dot{\theta}_v \end{pmatrix} = \begin{pmatrix} \frac{r\cos\theta_v}{2} & \frac{r\cos\theta_v}{2} \\ \frac{r\sin\theta_v}{d} & \frac{r\sin\theta_v}{d} \\ \frac{r}{d} & \frac{-r}{d} \end{pmatrix} \begin{pmatrix} \omega_L(t) \\ \omega_R(t) \end{pmatrix} \tag{1.22}$$

For control purposes the relation between the reference velocity in the plane $(\dot{x}_r, \dot{y}_r)$ and the reference velocity in the robot reference frame is required. To overcome the instantaneous limits imposed by system structure it is commonly chosen to control the velocity of a point that is not on the revolution axes of the wheels but that is slightly moved along the normal passing through the central point of the robot, see Fig. 1.4. The reference mapping between the two reference frame has the form:

$$\begin{pmatrix} v(t) \\ \omega(t) \end{pmatrix} = \begin{pmatrix} \cos\theta & \sin\theta \\ \frac{-\sin\theta}{b} & \frac{\cos\theta}{b} \end{pmatrix} \begin{pmatrix} \dot{x}_{ref} \\ \dot{y}_{ref} \end{pmatrix} \tag{1.23}$$

where b is the controlled point offset with respect to the revolution axis of the wheels. The simplest mapping technique for the control of mobile platforms involves the definition of a rate control scheme as presented in (1.14). A feedback force F_m proportional to the magnitude of the reference velocity is fed back to the human operator in order to give a measure of the velocity imposed on the robot:

$$F_m = k_{rate}(X_m - X_\omega) \tag{1.24}$$

with k_f the feedback factor. This signal superimposes with all other force feedbacks that the system and the interaction with the environment can produce, therefore a suitable force feedback range in the haptic device would be required for the implementation of this kind of control schemes.
A similar common mapping technique for the teleoperation of mobile robots is the definition of an impedance like relation between the motion of the master and the imposed reference velocity $(\dot{x}_{ref}, \dot{y}_{ref})$ to the slave. The master handle is modelled as a spring damper system characterized by a fixed mass m subject to a viscous force F_v in the environment and connected to the master reference frame by a spring generating an elastic force F_{el}. This way the acceleration imposed to the robot is obtained according to:

$$\ddot{X}_s = \frac{-F_v + F_{el}}{m} \tag{1.25}$$

where

$$F_v = b_{visc}\dot{X}_h \tag{1.26}$$

and

$$F_{el} = k_{el}(X_h - X_m) \tag{1.27}$$

The reference velocity is then obtained by integrating the acceleration signal with respect to time. A feedback force proportional to the elastic force generated by the spring is fed to the user as a measure of the level of acceleration applied.
Another solution [22] considers the definition of a virtual space in which the haptic reference pose is defined as a virtual mass that dynamically changes its position according to the behaviour imposed to the master device. In particular the velocity of the virtual mass $\dot{X}_v$ is commanded as:

$$\dot{X}_v = k_v X_m \tag{1.28}$$

with k_v the ratio between the maximum displacement of the haptic device and the maximum velocity of the mobile base. A linear spring connecting the virtual mass and the mobile robot generates the elastic force that imposes the acceleration reference to the slave device, that is considered immersed in a viscous environment, see Fig. 1.5. This leads to the definition of a control equation of the form (1.25). A similar

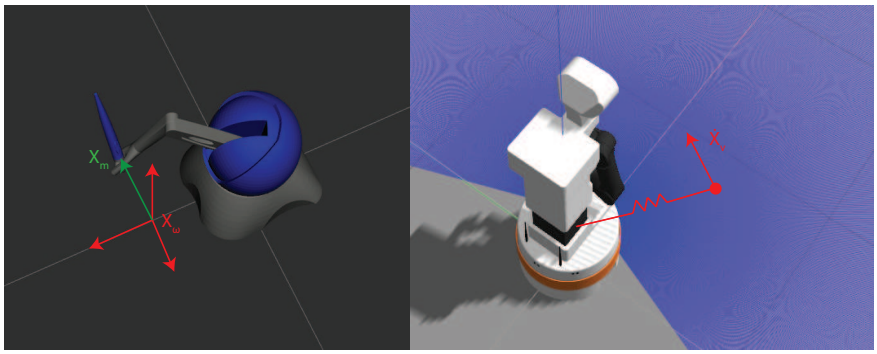

FIGURE 1.5: Velocity imposed to the virtual mass by means of the haptic device.

feedback proportional to the distance of the mobile robot to the virtual mass is produced. It is interesting to consider how the feedback force defined in this case is not directly correlated to the motion of the master but is instead related to the motion direction of the robot. This could lead to non zero feedback values even when the master device is producing a zero reference (the mobile base could still be reaching the virtual mass position).

1.3 An overview on Shared control

The first studies on shared control can be traced back to the 90's, when the scientific community was experiencing wide debates on the interrelation between humans and automation in the control loop. In the 1990 Norman was already stressing the importance of keeping the human operator inside the loop, by having a continuous interaction the could allow to act and prevent undesired result even in the worst case scenario[23]. In addiction several different studies were considering the importance for the human to be considered a part of the automation system in design phase to allow a good understanding and communication between the operator and the system itself, thus reducing the chance of unexpected behaviours and disagreement on each side [24] [25] [26]. This kind of approach have not always met high consensus in the practical field because of the annoyance and increased workload that at the

time the human operator had to experience. In addition it was difficult the define a formal appropriate level of automation (LoA) [27], or in other words the appropriate trade-off between human action and automatic behaviours of the robotic system. More recent studies are now focusing on the need to define a natural way to dynamically change the relation between the human and the robotic system to produce a flexible interaction [28] [29]. Many other studies in different fields have investigated shared control techniques related to vehicle control [30] [31] [32] [33] [34] [26], learning and skill transfer [35] and robotic surgery [36] [37].
In 2010 Abbink and Mulder [26] define shared control as "..a method of human automation interaction that allows both the human and the automation to exert forces on a control interface, of which its output (its position) remains the direct input to the controlled system.." Shared control can then be defined as a control structure that allows the cooperation of the operator with the system, that is characterized by some level of automation and that can provide assistance to the operator reducing the workload and the complexity of the task at hand. In [17] the authors have conducted a series of tests whose results proved that adding shared control to the system clearly improved the overall performances. Four guidelines have been defined for the definition of the interaction between the human operator and the automated system [38]:".. The operator should:

- always remain in control, but eventually experience or initiate smooth shifts between levels of automation
- receive continuous feedback about the automation boundaries and functionalities
- continuously interact with the automation
- benefit from increased performance and reduced workload.."

1.3.1 Shared control algorithms

The first work on shared control can be considered the study of virtual fixtures [36], abstract sensory information overlaying the feedback signals produced by the interaction of the slave device with its environment. The approach consisted in generating repulsive feedback forces used to prevent the operator to enter forbidden or dangerous regions of the environment. The first conception was considering rigid planar surfaces, extended later by other works considering an alternative design in which virtual forces were used to guide the human operator along the optimal trajectory, pulling him back in case of any deviation [39] [40] [41] [42]. These solutions where considering impedance surfaces, able to increase the operator performance up to 70%. The possibility to modify the rigidity of the surfaces allowed to impose very different behaviours:

- A rigid surface gives the automated system full control over the forbidden regions, preventing undesired behaviour but reducing the possibility for the operator to modify the predefined path;
- A very elastic surface could allow the operator to freely modify the intended trajectory on the expense of an increase of undesired errors or dangerous behaviours;

- An impedance surface could dynamically modify its behaviour, from time to time reducing or increasing the human determinism in the control structure.

This variety of behaviours promoted several studies on the optimal level of haptic authority (LoHA) [26] [33] [43] to be provided to the system.
Blending methods [44] can be considered as an attempt to close the gap between methods with high level of automation and little user control and methods where the operator is given high freedom at a higher psychological burden. The commands generated by both the system and the human are considered as two independent sources merged by some arbitration function that defines the relative contribution of each signal. Because of the computational simplicity and the performance they can bring, blending methods are currently one of the most used techniques in shared control approaches. Nevertheless this family of methods still presents some unsolved issues and is prone to possible failure [45]. New control paradigms are now focusing on handling the operator and system signal in a unified way, exploiting the user action to optimize the robot function [43]. This idea will be followed also in the first study proposed in this work, as will be presented in the next chapter.

Chapter 2

Shared control for liquid manipulation

2.1 Motion control for liquid vessels

This first chapter will consider a shared control strategy for the haptic control of a robotic manipulator interacting with liquid filled containers. The results obtained in this work have lead to the production of a scientific paper presented at Intelligent Robot and Systems (IROS 2018) [46]. The manipulation of complex shaped objects is a research field that requires the contribution of several different disciplines as mathematics, control, vision and robotics. This multiplicity has led to the development of many different solutions, capable of analyzing many aspects under different assumptions. Nevertheless the majority of the studies share their focus on three main problems:

- **The pose estimation of the object**: the pick and place operation requires a correct estimation of the position and orientation of the object in the operational space of the manipulator, in order to check feasibility constraints and allow the evaluation of the best pose for the robotic manipulator;
- **The resolution of the inverse kinematic problem**: the motion law for the robotic arm should be evaluated and optimized once the desired pick pose has been chosen;
- **The control of the object dynamic**: during the motion some objects might be subjected to vibration modes or particular orientations that could determine undesired interactions with the environment.

Among all the studies that concern the control of the object dynamics, the manipulation of liquid-filled vessels is still an active field of research, both in the domotic and in the industrial environment. New applications that consider assistive robots for indoor unstructured environment still suffer for the efficiency of the manipulation; in particular the spilling of the liquid that could be caused by the movement of the robot still impose the adoption of excessively slow dynamics. The same problem gains even more importance in the industrial environment, where the spilling of high temperature fluids could damage the mechanical structure of the kinematic chains and could pose a treat for the surrounding elements.
Among all the algorithm for sloshing suppression, feed-forward methods play a central role because of the complexity of measurements and high cost maintenance of electric sensors. Many different solutions rely on the application of input shaping

techniques and/or trajectory filtering and smoothing [47] [48] [49] [50] [51]. Another common approach considers the control of the tilting angle in order to prevent the liquid sloshing [52] [53]. Some other works are instead based on the optimization of the controlled trajectory, considering several constraints as acceleration and velocity. [54] [55] [56]. Several works have also considered the addition of a feedback compensation term based on the H^{∞} loop [47] [57]. Each of these studies have obtained quite satisfactory results in reducing the sloshing dynamics, but are still affected by some several issues among which an high strictness on the working hypothesis and in many case also robustness to error in parameter modelling. More recent studies are focusing on the control of entire robotic arms and are developing hybrid approaches that try to merge together different techniques. In [51] [50] for example the application of both a feed-forward approach as the input shaping technique and a tilting angle compensation is considered. The new approach proposed in this work follows the same line of thoughts and is based on the previous works of Prof. Biagiotti and Dott. Moriello [58] [59] In their previous paper they developed an exponential smoother to suppress the oscillations of the liquid, modelled as mechanical vibrations [58]. The algorithm was furtherly improved by the addition of a proper reorientation of the liquid vessel according to the imposed acceleration [59]. This work exploits the same concept by applying a trajectory filtering and an acceleration compensation by means of a proper reorientation of the vessel. The system defined this way does not required any information on the trajectory imposed and allows real time trajectory generation as the one obtained for example by an haptic device. A new plug-in component, that could be posed between the control layer and the actuator system and exploited in any liquid vessel control application, has been developed and tested. Particular attention has been brought to the teleoperation system, with the aim of reducing the complexity of the task for the human operator, determining an overall increase in the the operator performance. In this first study only the manipulation actuated by a robotic arm has been considered. The extension to the mobile manipulator case requires additional studies on the vibrations induced by the motion of the base and is still under development.

2.2 Modelling of the liquid

In this section the development of the equivalent mechanical model of the liquid vessel will be described. Let's consider a simplified scenario where the container is moved on a plane and it is rotated around an axis perpendicular to the plane itself. In this situation the dynamical behaviour of the system can be described by an equivalent mechanical model characterized by a fixed mass m_0 and a series of pendulums characterized by mass m_j, lenght l_j and support point placed along the normal to the surface passing through the fluid's baricentre at a distance L_j from the surface itself as shown in Fig. 2.1.
The pendulums defined this way are used to model the sloshing modes of the system. For control purposes just the first asymmetric mode, characterized by a single pendulum of mass m, length l and pivot posed at the center of the liquid surface is considered. It will also be assumed for the pendulum to be always perpendicular to the liquid surface, which is supposed to be flat, see Fig. 2.2.

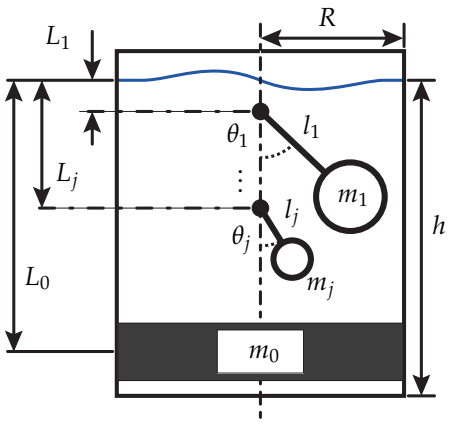

FIGURE 2.1: Equivalent mechanical model approximating the liquid dynamics in a cylindrical vessel.

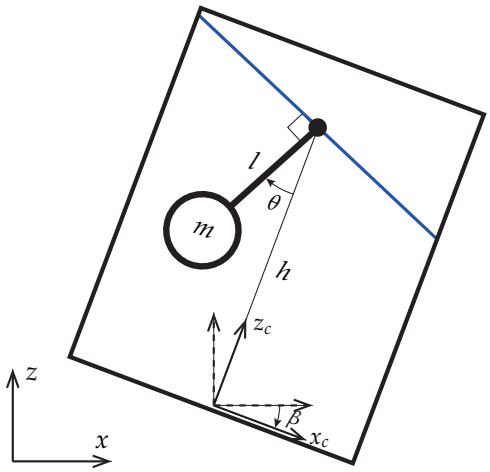

FIGURE 2.2: Simplified mechanical model approximating the first asymmetric sloshing mode in a cylindrical vessel.

The position of the pendulum mass is described by:

$$\begin{aligned} x_m &= x_c - h\sin(\beta) + l\sin(\beta+\theta) \\ z_m &= z_c + h\cos(\beta) - l\cos(\beta+\theta) \end{aligned}$$

where (x_c, z_c) define the position of the container with respect to the external base frame, the angle θ represents the rotation of the pendulum and β is the tilt angle imposed to the container, having its center of rotation along the centreline at distance h from the pendulum pivot. The dynamic of the system can be described using the Lagrangian equations.
The kinetic energy of the system is then defined by:

$$\begin{aligned} K &= \frac{1}{2}m\left[\dot{x}_m^2 + \dot{z}_m^2\right] \\ &= \frac{1}{2}m\Big[\left(\dot{x}_c - h\cos(\beta)\dot{\beta} + l\cos(\beta+\theta)(\dot{\beta}+\dot{\theta})\right)^2 \\ &\quad + \left(\dot{z}_c - h\sin(\beta)\dot{\beta} + l\sin(\beta+\theta)(\dot{\beta}+\dot{\theta})\right)^2\Big] \end{aligned} \tag{2.1}$$

Its potential energy is equal to

$$\Phi = m\,g\,z_m = m\,g\,(z_c + h\cos(\beta) - l\cos(\beta+\theta))$$

where g is the gravity constant. The Lagrangian, defined as $L = T - V$ and evaluated with respect to the angle θ is then obtained:

$$\begin{aligned} l\ddot{\theta} + \big(l - h\cos(\theta)\big)\ddot{\beta} - h\sin(\theta)\dot{\beta}^2 + \\ + \cos(\beta+\theta)\ddot{x}_c + \sin(\beta+\theta)\big(g + \ddot{z}_c\big) + \frac{b}{ml}\dot{\theta} = 0 \end{aligned} \tag{2.2}$$

The dissipative term $\frac{b}{ml}\dot{\theta}$ represents the damping force between the liquid and the container.
Let initially assume that the container is not rotating and $\ddot{\beta} = \dot{\beta} = \beta = 0$. The dynamic equation than takes the form:

$$l\ddot{\theta} + \frac{b}{ml}\dot{\theta} + \cos(\theta)\ddot{x}_c + \sin(\theta)\big(g + \ddot{z}_c\big) = 0 \tag{2.3}$$

where x_c, z_c are the external inputs and the equilibrium point

$$\theta = -\arctan\left(\frac{\ddot{x}_c}{g + \ddot{z}_c}\right) \tag{2.4}$$

is stable for $-\frac{\pi}{2} < \theta < \frac{pi}{2}$. In this situation a translational motion in the plane produces a pendulum swing that depends on the imposed acceleration and tends to the value (2.4). By linearizing the equation around $\theta = \dot{\theta} = 0$ and $\ddot{x}_c = \ddot{z}_c = 0$ the equation takes the form:

$$l\ddot{\theta} + \frac{b}{ml}\dot{\theta} + g\theta = -\ddot{x}_c, \tag{2.5}$$

which is equivalent to the second order equation:

$$\ddot{\theta} + 2\delta\omega_n\,\dot{\theta} + \omega_n^2\theta = u \tag{2.6}$$

where the parameters ω_n and δ depend on the characteristics of liquid and container, and the input u is proportional to the accelerations along the x axis. As usual for a pendulum

$$\omega_n^2 = \frac{g}{l}. \tag{2.7}$$

By applying residual vibration suppression theory for mechanical system it is possible to define a filter that shapes the input u to reduce the oscillation θ induced to the liquid. If also the rotation of the container β is considered, by assuming that $\theta = \theta_0 = 0$ in (2.2) the term $h\sin(\theta)\dot{\beta}^2$ becomes negligible. Moreover if the rotation center of the container is defined at the same distance l from the surface of the pendulum mass also $(l - h\cos(\theta))\ddot{\beta} \approx 0$. The dynamic equation derived has then the following form:

$$l\ddot{\theta} + \frac{b}{ml}\dot{\theta} = -\cos(\beta)\ddot{x}_c - \sin(\beta)\big(g + \ddot{z}_c\big) \tag{2.8}$$

By acting on β it is possible to enforce $\ddot{\theta} = \dot{\theta} = 0$, and therefore $\theta \equiv 0$, imposing that the second member of (2.8) is zero. To this purpose, the angle β must be chosen as

$$\beta = -\arctan\left(\frac{\ddot{x}_c}{g + \ddot{z}_c}\right). \tag{2.9}$$

2.3 Sloshing suppression

The generalization of the proposed modelling to the 3D case is straightforward. The reference signal, defined by $p(t) = [x(t), y(t), z(t)]^T$, is filtered to suppress the residual vibrations induced by the sloshing modes described by (2.5). In particular a damped harmonic smoother [60] has been chosen because of its interesting properties. The dynamic filter, proposed in Fig. 2.3, is characterized by a two-impulse input

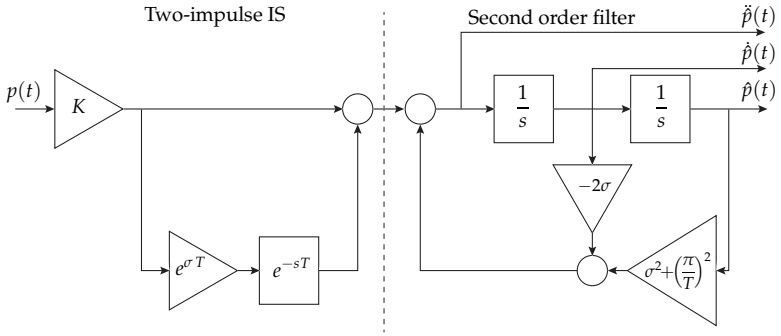

FIGURE 2.3: Harmonic smoother structure with constant $K = \dfrac{\sigma^2 + \left(\frac{\pi}{T}\right)^2}{1 + e^{\sigma T}}$.

shaper and a second order low pass filter, described in the Laplace domain by the following analytical expression:

$$H(s) = \frac{\sigma^2 + \left(\frac{\pi}{T}\right)^2}{1 + e^{\sigma T}} \frac{1 + e^{-sT} e^{\sigma T}}{(s - \sigma)^2 + \left(\frac{\pi}{T}\right)^2}. \tag{2.10}$$

The smoother is characterized by the two constant parameters T and σ. In Fig. 2.4 is possible to analyze the impulse response according to the different values assigned. The parameter T defines the duration of the impulse response and the overall delay produced on the filtered signal with respect to the original one, whereas σ characterizes the shape of the response.
The zero-pole map of the smoother is proposed in Fig. 2.5. The cancellation of the sloshing dynamic can be obtained by imposing:

$$\sigma = -\delta\omega_n, \qquad T = \frac{3}{2}\frac{2\pi}{\omega_n\sqrt{1 - \delta^2}}. \tag{2.11}$$

The smoother works as an input shaper but with respect to a ZV (Zero Value) input shaper it produces a delay of triple value.
On the other end it presents several advantages that overcome the additional induced delay:

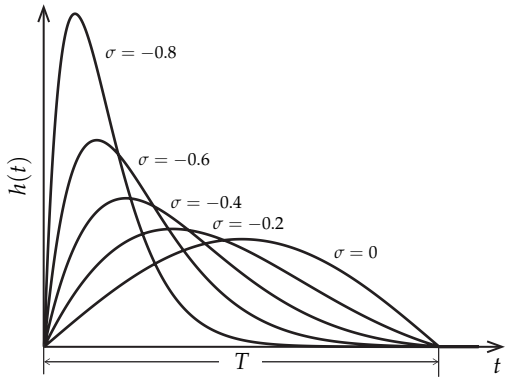

FIGURE 2.4: Impulse response of the damped sinusoidal filter $H(s)$ for different values of σ.

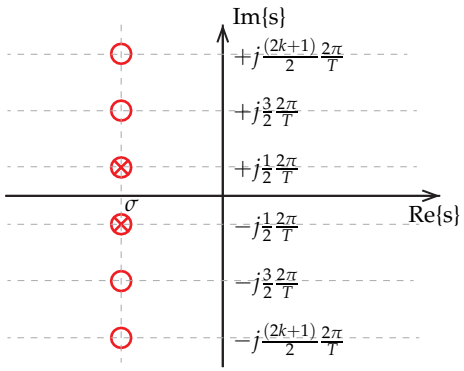

FIGURE 2.5: Pole-zero map of the damped harmonic smoother $H(s)$: σ and T are the free parameters that appear in (2.10).

- The filter increases the level of smoothness of the reference signal guaranteeing the output signal to belong to the C^2 class and therefore having continuous velocity and acceleration (provided the continuity of the original signal)
- The structure of the filter, expressed in the controllable canonical form, allows also the evaluation of the 1^{st} and 2^{nd} derivatives of the produced output in realtime.
- The low pass characteristic, proposed in Fig. 2.6, guarantees the suppression of the high slosh modes.

It is worthwhile to consider that $|H(j\omega)|$ is proportional to the percentual residual vibration induced by the filtered signal when the resonant plant is completely undamped and the resonant frequency is affected by an estimation error. This way $|H(j\omega)|$ can be seen as a measure of the robustness of the filter. In Fig. 2.6 is clearly shown that the modes characterized by $w_n > 3\frac{\pi}{T}$ are reduced even if the evaluation of w_n is not exact.

The filtered signal $\hat{p}(t) = [\hat{x}(t), \hat{y}(t), \hat{z}(t)]^T$ is used to define the orientation of the manipulator in each time instant. The container should in fact be rotated in such a way to be aligned with the equilibrium angular pose caused by the acceleration to the virtual pendulum. The angular configuration of the pendulum, proposed in Fig. 2.7,can be fully described in spherical coordinates by the lenght of the pendulum l

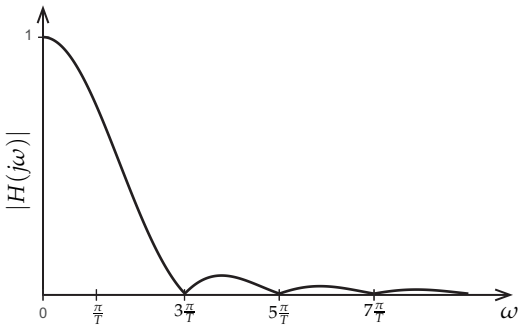

FIGURE 2.6: Magnitude of the frequency response of the damped sinusoidal filter $H(s)$ with $\sigma = -0.0431$ and $T = 0.7211$s.

and the two angles ϕ and θ. In [59] the dependency of these angles from the linear acceleration imposed to the vessel has been analytically deduced, i.e.

$$\theta = \tan^{-1}\left(\frac{\sqrt{\ddot{x}^2 + \ddot{y}^2}}{g + \ddot{z}}\right) \tag{2.12}$$

$$\varphi = \pi + \text{atan2}\ (\ddot{y}, \ddot{x}) \tag{2.13}$$

where atan2 is the four quadrant inverse tangent. The robot manipulator must rotate the vessel about the point where the mass m is located at rest in order to impose the orientation given by (θ, φ). Therefore, two consecutive rotations $\text{Rot}_z(\varphi)$ and $\text{Rot}_y(-\theta)$ must be applied. Moreover, since the first rotation about the z axis would cause an undesired vessel rotation of an angle φ about its symmetry axis, it is necessary to add the converse rotation about the z axis after the $\text{Rot}_y(-\theta)$. Finally, the desired configuration of the vessel is

$$\mathbf{R}(\theta, \varphi) = \text{Rot}_z(\varphi)\,\text{Rot}_y(-\theta)\,\text{Rot}_z(-\varphi). \tag{2.14}$$

It is worth to noticing that the term $\text{Rot}_z(-\varphi)$ offers an additional advantage when $\ddot{y} = \ddot{x} = 0$. In this case, the angle φ in (2.13) is not well defined; however, since $\theta = 0$, $\mathbf{R}(\theta, \varphi) = \text{Rot}_z(\varphi)\,\text{Rot}_z(-\varphi) = I_3$, being I_3 the $3-\text{by}-3$ identity matrix.

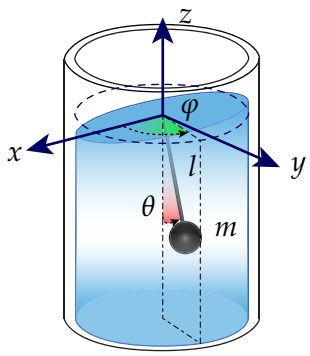

FIGURE 2.7: Spherical pendulum modelling the sloshing dynamics in a liquid-filled vessel that moves along a 3D trajectory.

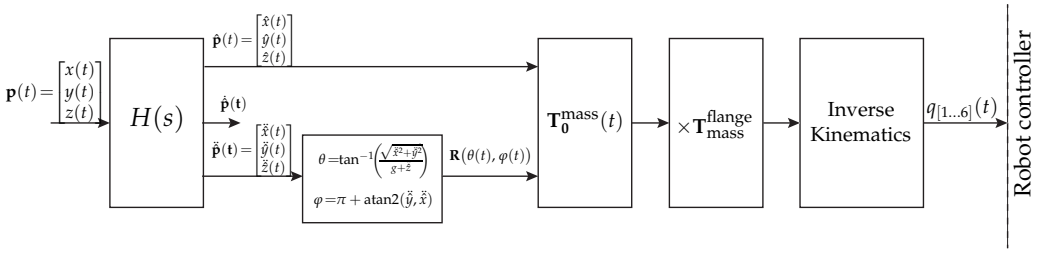

FIGURE 2.8: Feed-forward controller for sloshing compensation based on the harmonic smoother.

By considering the expressions of θ and φ that appear in (2.12) and (2.13) and are used to define the instant value of the rotation matrix $\mathbf{R}(\theta,\varphi)$ defining the orientation of the vessel, the benefits of the harmonic smoother, that guarantees the continuity of the accelerations for any kind of input (supposed continuous) and allows their computation online, are evident.
The complete structure of the proposed feed-forward controller for robust sloshing compensation with unknown reference signal is illustrated in Fig. 2.8. The filtered trajectory $\hat{\mathbf{p}}(t)$ and the rotation matrix $\mathbf{R}(\theta(t),\varphi(t))$ are organized in the homogeneous transformation matrix

$$\mathbf{T}_{\mathbf{0}}^{\text{mass}}(\mathbf{t})=\begin{bmatrix}\mathbf{R}(\theta(t),\varphi(t)) & \hat{\mathbf{p}}(t)\\ 0\quad 0\quad 0 & 1\end{bmatrix}$$

that provides the desired configuration of the reference frame attached to container with respect to the world reference frame. In order to take into account the relative pose of the container with respect to the robot flange $\mathbf{T}_{\mathbf{0}}^{\text{mass}}(\mathbf{t})$ is multiplied by the constant matrix $\mathbf{T}_{\text{mass}}^{\text{flange}}$, i.e.

$$\mathbf{T}_{0}^{\text{flange}}(\mathbf{t})=\mathbf{T}_{\mathbf{0}}^{\text{mass}}(\mathbf{t})\cdot\mathbf{T}_{\text{mass}}^{\text{flange}}.$$

Finally, the instant configuration of the robot flange $\mathbf{T}_{0}^{\text{flange}}(\mathbf{t})$ is processed using the inverse kinematics to derive the joint trajectories $q_{[1...6]}(t)$ that the robot manipulator must track.

2.4 Experimental tests

The experimental setup developed to test the performance of the proposed method is shown in Fig. 2.9 The system has been designed according to a master-slave teleoperations setup. The operator motion in the 3D space is tracked by a Vicon system (Vicon, Oxford, UK), elaborated in the main workstation and sent through the network to a Comau Smart Six anthropomorphic robot acting as slave device. On the master side the set of 8 Bonita cameras were operating at their maximum frequency (250 fps) with a 2 ms latency. A visual feedback of the slave motion was provided on an apposite screen for monitoring purposes only. On the slave side a pc running RTAI-linux 3.9 operating system on a Ubuntu NATTY distribution with Linux kernel 2.6.38.8. allows the communication between the main workstation and the robot

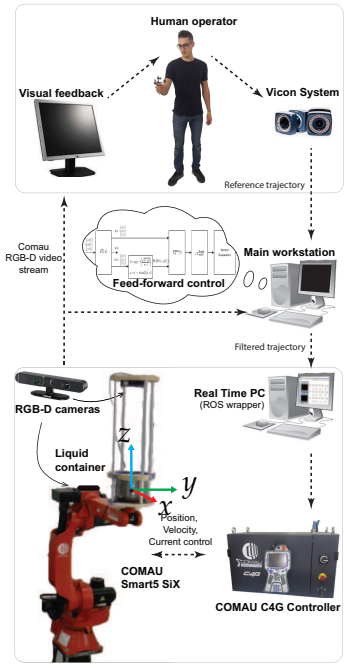

FIGURE 2.9: Experimental setup.

controller. A steel pot (of radius 97.5 mm) has been connected to the flange of the slave and filled with 3 liters of water. During the execution of the test the liquid surface has been monitored by an ASUS Xtion PRO Live RGB-D camera mounted on a specifically-designed support above the filled container. IN order to simplify the surface detection a blue pigment has been added to the water. Another RGB-D camera mounted on top of the robot third joint would provide visual feedback to the master side. All the communication has been handled through the Robotic Operating system (ROS) kinetic distribution running on Ubuntu 16.04. A purposedly built wrapper, base on he "C4G OPEN" software functionality of the Comau controller allowed the communication with the slave robot. The 3D real time position signal of the operator is tracked by the cameras, filtered and sent to the robot controller without any feedback in the loop. The filter acts as a shared control layer that entirely takes care of the sloshing suppression, simplifying the task of the user. The recorder trajectories are implemented without any kind of modification or scaling operation. For safety reasons during the tests the robot workspace has been restricted to a box of $0.6 \times 1 \times 0.8$ meters (along x, y and z directions, respectively) centered around the operator initial position.

2.4.1 Test results

The harmonic smoother defined in (2.11) requires a correct estimation of the natural frequency and the damping ratio related to the sloshing. The value obtained for the setup previously defined equals to $\omega_n = 13.076$ rad/s, $\delta = 0.005$. For an addition insight on the evaluation of these parameters see [59].
The reorientation of the container is defined uniquely according to the translational acceleration of the container rotated around its symmetry axis at distance $l = 0.0574$ from the liquid surface, where l is the lenth of the virtual pendulum that models the

sloshing mode deduced from (2.7).

A preliminary set of tests have been carried out to evaluate the performance of the proposed technique with respect to straightforward reference tracking or orientation compensation only. In each test a predefined motion performed by the human operator were tracked and recorded, so that the same trajectory could be used to test the slave behaviour under different control paradigms.
In all the following graphs will be used a common notation for simplicity:

- The black dashed line represents the tracked motion of the human operator
- The red line represents the trajectory filtered by the harmonic smoother

In Fig. 2.10 a translation motion along the y axis performed several times is presented.

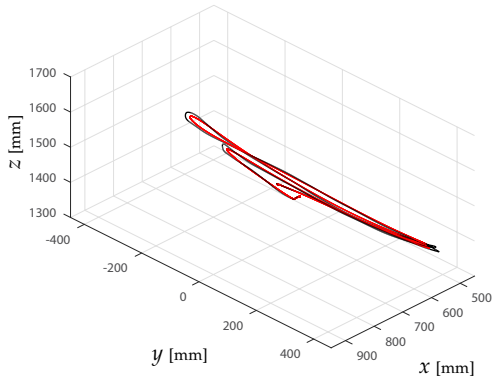

FIGURE 2.10: Geometric path of a linear movement of the user tracked by the motion capture system. The black line is the original trajectory while the red line represents the trajectory filtered by the harmonic smoother.

The corresponding motion profiles with respect to time are shown in Fig. 2.11.

Also the acceleration profiles are proposed here because of their significance for the application. In the unfiltered cases accelerations are obtained through numerical differentiation, leading to high peak valued and noisy signals due to the camera measurements and the tremors and small movements that characterize the behaviour of any human operator. As expected on the other hand the filtered signal is characterized by a very smooth trajectory at the cost of a small time delay that with respect to the previously defined values equals $T = 0.6895$ s.

The liquid response can be appreciated more in particular in Fig. 2.12, where the tilting angle θ of its surface, approximated to a plane, is analyzed under the different reference trajectories presented in Fig. 2.11 The evaluation technique to extract the angle data from the measurements of the 3D camera is furtherly explained in [59]. Fig. 2.12(a) presents the liquid response when the unfiltered trajectory is provided. Despite the smoothness of the motion profile a chaotic behaviour can be observed. A similar response can be seen in Fig. 2.12(b) because of the implementation of the reorientation of the vessel. In addition also a chaotic behaviour can be noticed on the liquid surface probably due to the high noise in the acceleration profiles (see Fig. 2.11(b)) that excite high order sloshing modes via the angular compensation.

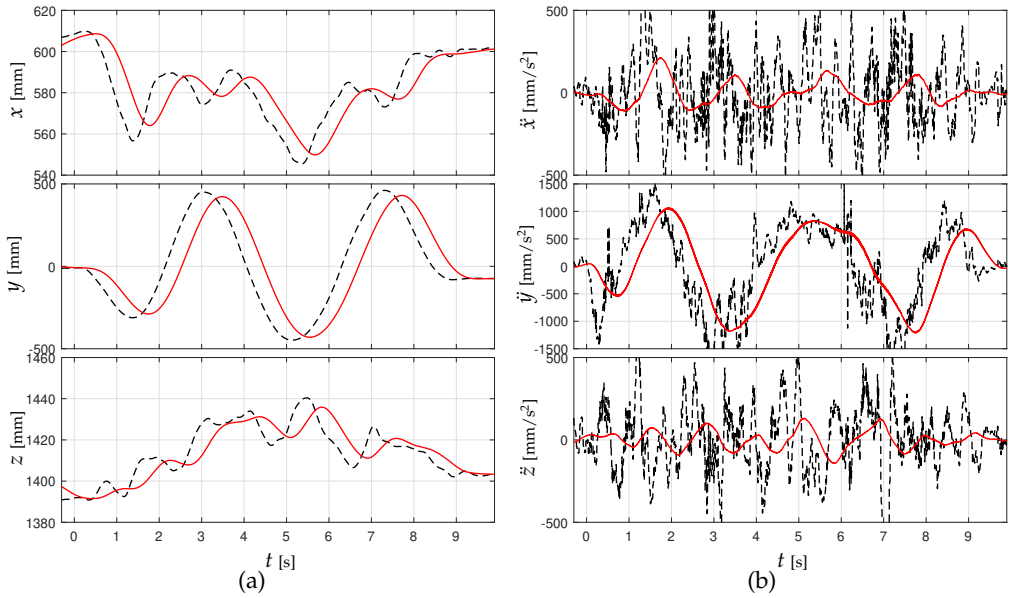

FIGURE 2.11: Motion profiles corresponding to the geometric path of Fig. 2.10: positions (a) and accelerations (b). The black dashed lines are related to the original motion while the red solid lines represent the filtered trajectory.

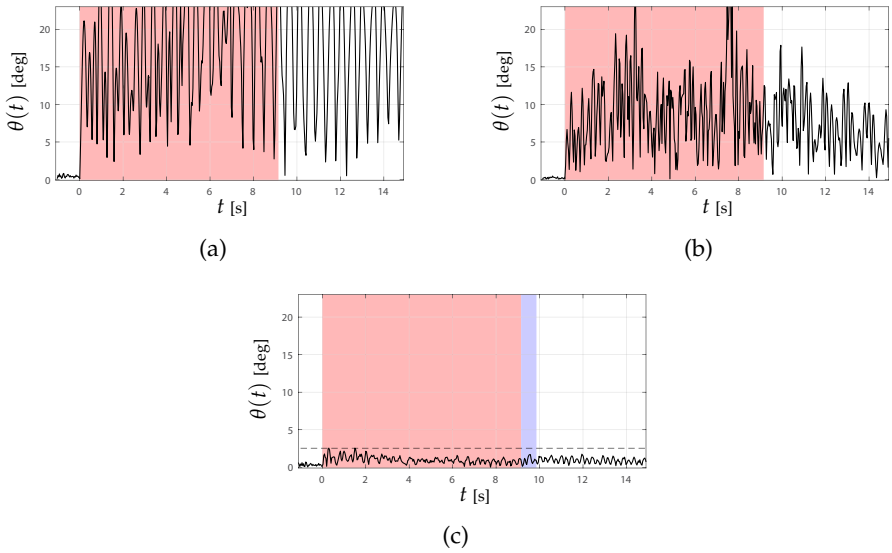

FIGURE 2.12: Sloshing angle profiles measured when the liquid vessel is moved according to the trajectories of Fig. 2.11: unfiltered trajectory (a); unfiltered trajectory with orientation compensation (b); smoothed trajectory with orientation compensation (c). The red area indicates the motion time while the blue area highlights the time lag T introduced by the filter.

In fact in this situation the hypothesis of a planar surface for the liquid does not hold anymore and the whole evaluation brings misleading results. On the other hand the effective sloshing reduction after the implementation of the proposed filter

is clearly visible in Fig. 2.12(c). In particular the sloshing angle theta presents a reduced range of variation both at steady state and during the motion that do not exceeds 2.5 degrees.

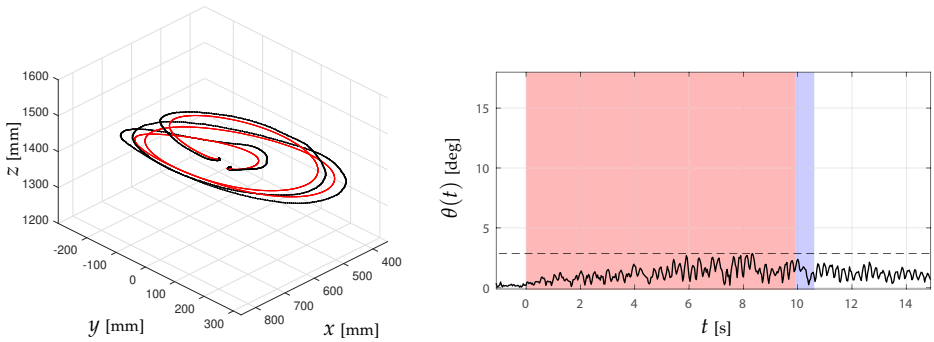

(a) (b)

FIGURE 2.13: Geometric paths disposed on the plane $x - y$ used to test the proposed algorithm (a) and resulting sloshing angle θ (b).

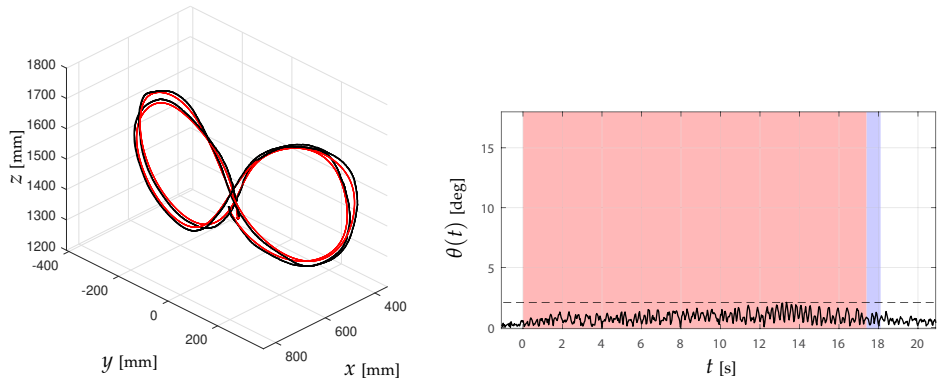

(a) (b)

FIGURE 2.14: Geometric paths disposed on the plane $y - z$ used to test the proposed algorithm (a) and resulting sloshing angle θ (b).

Similar results can be observed when the motions are performed on the horizontal plane $x - y$, see Fig. 2.13, or in the vertical plane $y - z$, see Fig. 2.14. These examples can show very clearly the rather limited deformation caused by the smoother. Additional experiment have been performed online, with an approximate duration of one minute and reaching a maximum acceleration higher than 1 m/s^2. All the test carried out have shown that the filtering causes a sloshing angles that does not exceed 8 degrees, proving the effectiveness of the proposed approach.

2.5 Conclusions

In this work a new shared control technique for the manipulation of liquid-filled container has been developed. This work has enhanced the idea proposed in [59] removing the requirement of the a priori knowledge of the reference trajectory. The

improvement has been possible thanks to the characteristics of the damped harmonic smoother, that provides also the acceleration profile of the filtered trajectory, allowing the evaluation in real time of the proper reorientation for the container. The extensive tests have proved the effectiveness of the filter, that could allow the operator to easily manipulate liquid vessels without having to consider the consequence of each of its motion. The next step will consider the implementation and integration of the system in a mobile manipulator, where also the dynamics of the mobile base have to be taken into consideration.

Chapter 3

Real time trajectory planning for haptic assistance

3.1 Planning exploiting B-spline properties

An important aspect of the control of a mobile manipulator is the definition of the trajectories imposed to the arm and the mobile base during the interaction with the environment. This becomes particularly important when the robot interacts in presence of other human or robotic assets or when relevant delays are present in the communication network. A real time dynamic planning strategy, able to automatically adapt to changes in the environment and to avoid dangerous situations at minimum computational cost, proves crucial for the task at hand. In addition an autonomous avoidance layer can provide safety for the interaction and could ease the task of the human operator, that can keep its focus on the current task exploited with the end-effector while the system autonomously takes care of the environment. The research of path planning algorithm has been a broad field characterized by many different contribution. A popular technique exploits the concept of retraction to build a roadmap, a set of collision free paths, that allow to check the connectivity of free configuration space and obtain the final path [61] [62] [63]. A similar result is determined through the application of sample based planner like A* where the cell decomposition of the environment allows to build a network of channels that can provide the same result [64] [65] [66] [67]. Another common strategy considers the application of heuristic methods exploiting the same network concept as probabilistic roadmaps [68] or a potential field driven environment like the the artificial potential planning[69] [70] [71]. Several other quite different techniques use the information obtained from the sensors of the platform to define the path to follow like navigation function on gridmaps [72] [73] or follow the gap algorithms [74] [75].

Despite the differences of solution all the techniques can be separated in two main categories:

- The global optimization algorithms that at an increased computational cost are able to find the optimal path to reach the predefined goal, provided its existence;
- The local heuristic algorithm that react to the environment in real time while the robot moves toward the target, but that can not guarantee the successful reachment of the target nor the optimality of the path.

The choice of the algorithms to apply usually is taken considering a trade-off between several factors as the computational cost, the level of reactivity required, the

complexity of the environment and the time constraints. This study aims at overcoming the difference between the two families and at defininining a new algorithm capable of providing a full geometry planning at low computational cost. The definition of the new algorithm has been based on a specific type of spline curves, the uniform B-spline.

3.2 The spline trajectory

A spline trajectory of degree d in the so-called B-form, in short B-spline, is a parametric curve characterized by the linear combination of some basis functions $B_j^d(t)$ of degree d and a vector of control points p_k that roughly defines its geometry:

$$q(t) = \sum_{k=0}^{n-1} p_k \, B_k^d(t), \qquad t_0 \leq t \leq t_{n-1}. \tag{3.1}$$

The basis functions, which are scalar functions of class C^{d-1} defined over a vector of time-instants $[t_0, t_1, \ldots, t_{n-2}, t_{n-1}]$, known as knots vectors, contain the temporal information that determines how the curve is followed and can be defined recursively as:

$$B_j^d(t) = \frac{t - t_j}{t_{j+d} - t_j} B_j^{d-1}(t) + \frac{t_{j+d+1} - t}{t_{j+d+1} - t_{j+1}} B_{j+1}^{d-1}(t) \tag{3.2}$$

with

$$B_j^0(t) = \begin{cases} 1, & \text{if } t_j \leq t < t_{j+1} \\ 0, & \text{otherwise.} \end{cases}$$

The chosen degree d of the basis function defines the interpolation behaviour and the smoothness of the curve: a degree $d = 1$ for example defines a linear B-spline characterized by a set of segments joining the control points. A degree $d = 3$ on the other hand produces a cubic B-spline that do not directly interpolate the control point vector but presents an higher degree of smoothness, see Fig. 3.1.

Since B-spline of order $d > 1$ do not interpolate the control point vector a new set of points imposing geometry conditions on the curve at certain time instants t_i must be defined:

$$q(t_i) = q_i^\star. \tag{3.3}$$

where q_i represent the imposed via points to be crossed by the curve. The control point can then be extrapolated from the via point by solving a linear system as explained in detail in [76].
It is important to notice that $B_k^d(t)$ is zero everywhere except in the time interval $[t_k, t_{k+d+1}]$, see Fig. 3.2. Therefore a variation of a control point p_k only affects the portion of the curve in the proximity of the modified point, see Fig. 3.3.

Of particular interest is a family of B-spline, the Uniform B-spline, characterized by an equally-spaced knot vector. This type of spline in addition to the already specified properties is characterized by basis functions that are consistent under time shifts:

$$B_{k+1}^d(t) = B_k^d(t - T), \qquad k = 0, \ldots, m - 2.$$

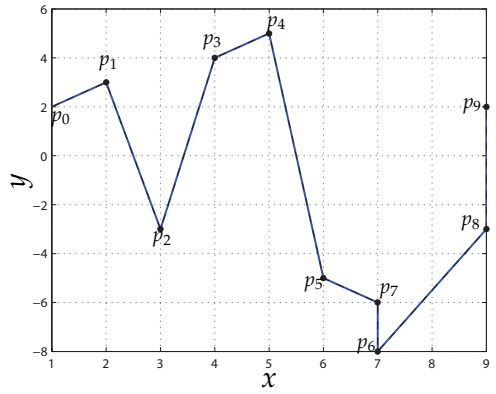

(a)

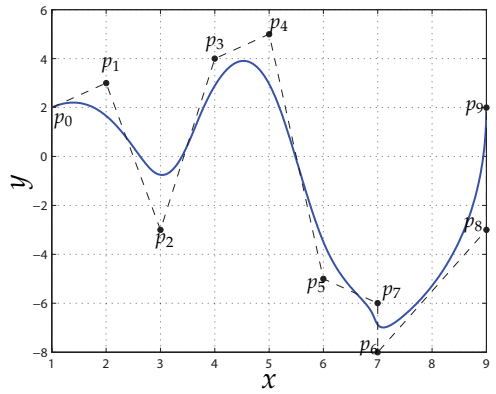

(b)

FIGURE 3.1: 2D B-spline curves: linear (a) and cubic (b).

This way each basis function can be evaluated in terms of the first basis function B_0^d:

$$B_k^d(t) = B_0^d(t - kT), \qquad k = 0, \ldots, m-1$$

and the overall spline can be rewritten as:

$$q_u(t) = \sum_{k=0}^{n} p_k B_0^d(t - kT), \qquad 0 \leq t \leq (m-1)T. \tag{3.4}$$

The trajectory defined this way can be efficiently generated, see [77], by the dynamic filter proposed in Fig. 3.4 . The system is characterized by a zero-order hold and a chain of d dynamic filters defind as:

$$M(z) = \frac{1}{N} \frac{1 - z^{-N}}{1 - z^{-1}} \tag{3.5}$$

that are fed by a set of impulses of amplitude p_k. The proposed trajectory generator was evaluated through the discretization of continuous-time dynamical filter in the form:

$$M(s) = \frac{1 - e^{-sT}}{Ts} \tag{3.6}$$

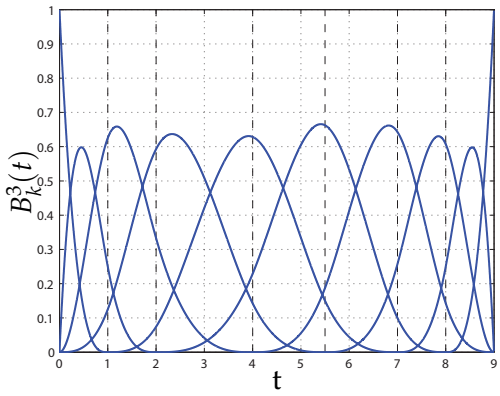

FIGURE 3.2: B-spline basis functions of degree 3 defined over the knots vector $[0,0,0,0,1,2,4,5.5,7,8,9,9,9,9]$ that form the B-spline of Fig. 3.1.

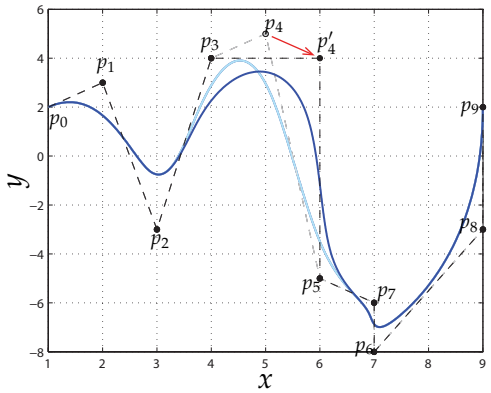

FIGURE 3.3: Local modification of a B-spline curve due to the change of position of a control point.

where $N = T/T_s$ as proposed in [77]. Since the scheme of Fig. 3.4 produces scalar B-spline a set of n filter is required for each component of the trajectory to be defined R^n.
Note that the use of the digital filter for B-spline generation offers the following advantages:

- a new value of the curve is provided at each sample time of the control loop;
- the continuity of the output curve is always guaranteed even if the control points position is modified;
- the computational burden is extremely low and the implementation process rather simple, since d FIR filters, whose input is kept constant to the value of the control points for a duration of T seconds, are sufficient for computing the trajectory.

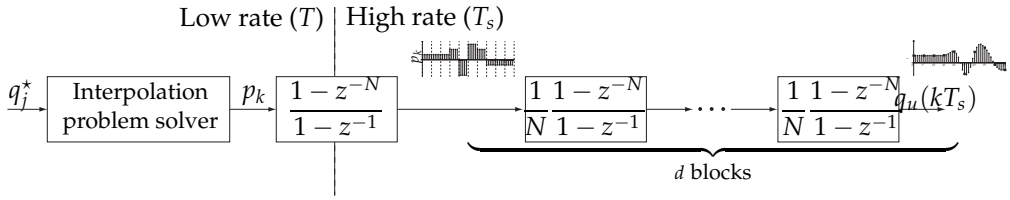

FIGURE 3.4: Structure of the discrete-time filter for B-spline trajectories planning.

This class of curves evaluated through digital filtering presents several interesting properties that make them the perfect tool to achieve a simple and reactive path planning:

- **Low curvature**: spline curves provides the lowest curvature among all the polynomial curve of the same degree, providing the smoother trajectory with lowest acceleration for the target motion
- **Continuity of acceleration**: spline of at least degree 3 belongs to C^2 and guarantees continuity of the curve up to the second derivative;
- **Real time evaluation**: the series of three FIR filters allows real time evaluation of the spline, by evaluating a new point of the trajectory for each control cycle of the motors;
- **Local modification** the motion of a point in the trajectory produces an effect only on the part of the curve close to the point itself;
- **The uniformity of knots** by defining the required pose at equally-spaced time instants and the period of the curve it is possible to directly define the motion law for the robot.

These characteristics allow the characterization of a curve, defined by a series of via points, that can produce a trajectory that could be locally modified because of changes in the environment without affecting the current motion of the robot.

3.3 A physical behaviour embodied in B-spline curve

The trajectory in the environment is obtained in each time step by evaluating the position of the via point defining the spline. It is possible then to consider each point in the curve as a virtual dynamic agent interacting with the environment and with its neighbours points in the line, allowing the trajectory to reactively shape itself in real time according to the environment changes. Each via point, as shown in Fig. 3.5, is characterized by a fixed mass and is connected by two identical springs to the previous and the following via point in the spline. In addiction each point is considered immersed in a viscous environment. This way the points are modelled as mass-spring-damper systems reacting to an external force and the point acceleration is obtained through:

$$F_{acc} = F_{visc} + F_{el} + F_{Ext} \tag{3.7}$$

that in the planar case can be defined as following:

$$m\ddot{p}_i + b\dot{p}_i + k(\tilde{p}_{i,i-1} - \delta) + k(\tilde{p}_{i,i+1} - \delta) = -\bigtriangledown \Phi(p_i) \tag{3.8}$$

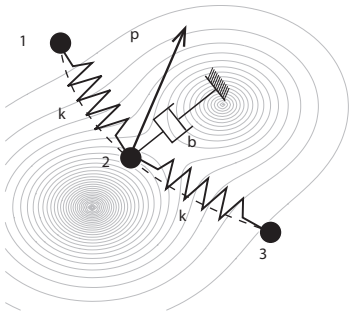

FIGURE 3.5: Via point as dynamical systems

where p_i represents the point position in the plane, m is the mass of the point, b is the viscosity of the environment, k is the spring coefficient, δ is the spring resting length and $\bigtriangledown\Phi$ is the repulsive force generated by the environment as explained in the next section.

3.3.1 Environment modelling

At first a simplified environment has been considered in order to explain and test the capabilities of the algorithm. The planar environment is characterized by obstacles of known dimension, that are modelled as circles centered in their baricentre and radius equal to the distance between the center itself and its furthest vertex.The environment is considered fully known a priori and all the obstacles are well separated from each other (two colliding obstacles are modelled by the same circle)Each obstacle generates a potential field inversely proportional to the distance from its center up to a certain distance. This way the via points are affected by a particular obstacle only within a certain distance from its border. It is interesting to observe that since the virtual agents could be, in some time instants, overlapping with the obstacles, the potential field generated does not reach the infinity value along the obstacle border like any artificial potential algorithm but instead keeps increasing its value toward the obstacle center.
Each obstacle is then characterized by:

- a center $o = (o_x, o_y)$
- a radius r
- a safety distance ρ from its border at which the potential reaches 0
- a potential value ϕ_b representing the potential value imposed at the obstacle border
- a constant parameter g_0 representing the gain at which the potential increase inside its surface.

The potential field generated this way is shown in Fig. 3.6 The total potential Φ acting on each agent p_i is given by the sum of the effects of all the potentials generated by the obstacles:

$$\Phi(p_i) = \sum_{k=0}^{l} \Phi_k(p_i) \tag{3.9}$$

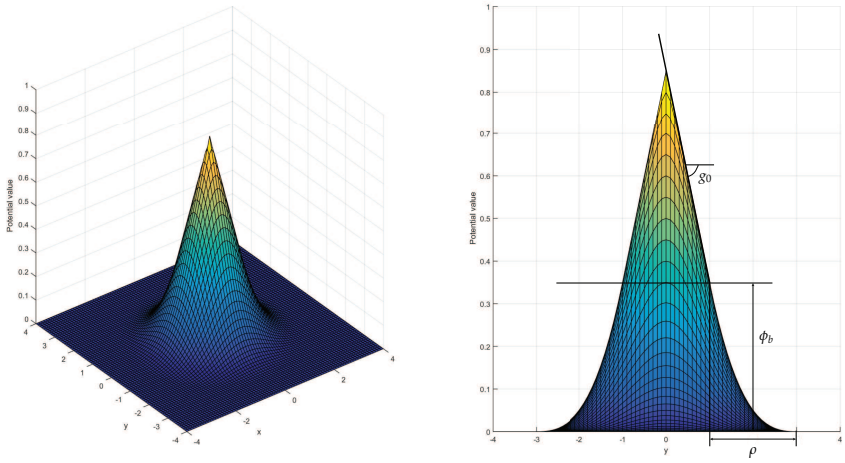

FIGURE 3.6: Potential field generated by a circular obstacle

where l is the number of obstacles and

$$\Phi_k(p_i) = \begin{cases} g_0(|p_i - o| - r) + \phi_b, & \text{if} |p_i - o| < r \\ f(p_i), & \text{if} r \leq |p_i - o| < r + \rho \\ 0, & \text{if} |p_i - o| \geq r + \rho \end{cases} \tag{3.10}$$

As shown in (3.10) the potential on the inside of each obstacle grows with inverse proportionality with respect to the distance from its center while on the outside decreases according to an exponentially decreasing function:

$$f(p_i) = \phi_b + g_0(|p_i - o| - r) - \frac{3\phi_b + 2g_0\rho}{\rho^2}(|p_i - o| - r)^2 + \frac{2\phi_b + g_0\rho}{\rho^3}(|p_i - o| - r)^3 \tag{3.11}$$

Since the potential of an obstacle acts on an agent only within a fixed radius from its surface, only the obstacles within a circular area of radius r are considered for the evaluation of the overall potential force applied in a particular time instant.

3.3.2 Advanced Environment modelling

The proposed modelling for the environment, despite its usefulness for testing purposes, describes poorly a real environment and all the different shapes that could be encountered during the robot interaction. A peculiar example could be the avoidance of a human arm that is operating at the border of the workspace of the controlled robotic arm. Because of this a more advance modelling, where some of the constraint previously imposed are relaxed, is required. Also in this case it will be presented the two dimensional case; the extension to the 3D one is straightforward. The environment is reconstructed as an occupancy grid. Each black pixel of the grid represents an occupied point in space. The total potential field acting on the agent is produced by all the occupied points in the grid within a fixed radius r from the agent itself

$$\Phi^{gr}(p_i) = \sum_{k=0}^{l} \Phi_k^{gr}(p_i) \tag{3.12}$$

where l is the number of occupied pixels and

$$\Phi_k^{gr}(p_i) = 1/(k - k_r) \tag{3.13}$$

Since the occupancy grid could not be fully known a priori the cells that have not been mapped yet are considered occupied for the purpose of the algorithm.

3.4 The global planner

The characteristics of the agents just defined interacting with the modelled environment allow to define a new typology of planners, able to evaluate at runtime and with low computational cost both the geometry of the splined shaped path and the motion law for the robot. Let's consider a fixed environment modelled as showed in section 3.3.1 and a mobile base that has to move from a starting point S to a goal point G. It is possible to define a straight line that connects S to G. Along the line n key points at the same distance from each other are identified. The number of points n is given by:

$$n = \frac{L}{\delta} - 1 \tag{3.14}$$

where L is the total length of the line and δ is the chosen rest length of the springs among the agents. The points obtained in this way are considered the virtual via points of the final trajectory. Once defined, the agents, as shown in Fig. 3.7, start interacting with each other and with the environment. In each time step Δ_t

- the obstacle repulsive force directs the via point immersed in the potential field to the border of its potential region
- the elastic forces between the agents prevent them from dispersion or from movement too far away from each other
- the viscous force reduces the transient motion in the zero potential region

Once the system has converged to steady state the final spline trajectory obtained will guide the robot along a path that keeps the minimum allowed distance from the obstacles and is able to reach the target. The trajectory evaluated this way can

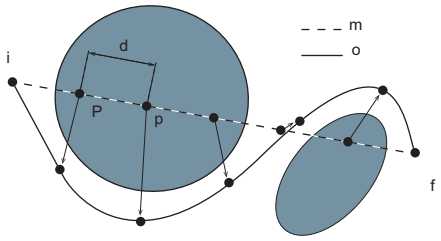

FIGURE 3.7: Working principle of the planner

be computed both offline or in real-time, with the motion of the robot allowed only after a certain degree of convergence of the agents' motion. Since the motion and the convergence of the agents is determined by frequency of update of the agents; setting a higher frequency with respect to the motion control of the base guarantees immediate convergence and evaluation. The proposed algorithm, as shown in

Fig. 3.7, is also able to overcome one of the main problems of potential-field base planners: the local minima problem. In fact even if one or more of the via points got stuck in a potential trap, the following one in the curve will be subject to different forces, leading the stuck agent away from the minima by means of the elastic force or simply allowing the robot to go through. Despite these characteristics some major drawbacks can be noticed:

- The motion of an obstacle could stretch the trajectory infinitely
- In case of a large distance to be covered, the number of agents could become noticeable
- Complex shaped obstacles could cause a fault in the algorithm

In order to overcome these issues an improved version of the algorithm is proposed.

3.5 The Pac-Man algorithm

Let's consider a dynamically changing environment with obstacle of generic shape. The new planning framework considers only a predefined number of agents. Because of this choice the curve is very likely not going to be able to reach the final goal G but only to cover a small portion of the total path. The final agent on the line, from now on called the explorer play plays a special role and its dynamic is modelled in a slightly different way: it is characterized by a single spring connecting it with the previous point and by a constant potential force that draws it toward the target. In addition each agent is assigned a different mass value, decreasing along the line as shown in Fig. 3.8 This way the agents exploit a different role:

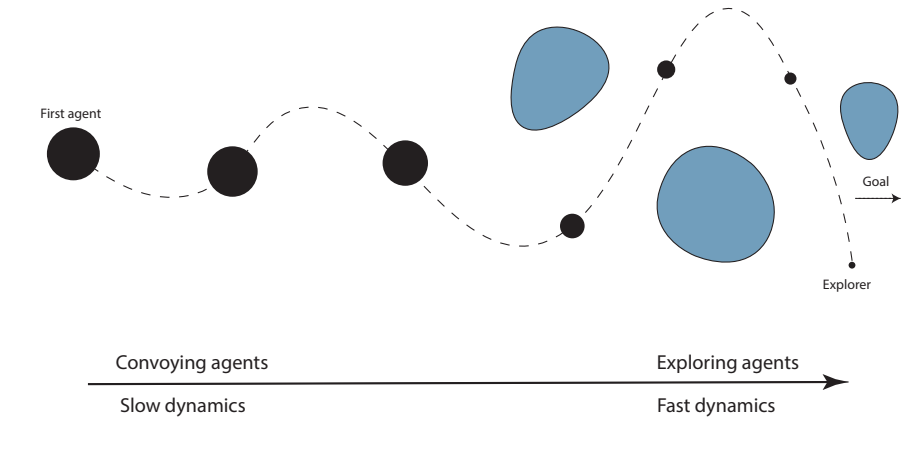

FIGURE 3.8: Agent mass distribution

- the agents closer to the robot, characterized by slower dynamics, act as convoyers, defining the final path for the robot
- the agents further from the robot, characterized by higher dynamics, act as explorers, reactively responding to changes in the environment

It is worth reminding that thanks to the B-spline characteristics the fast motion of the explorer agents is not perceived by the robot. In addition a higher update frequency of the agents with respect to the control frequency of the motors guarantees a steady state in each control time instants. To reach the final target a periodic reconfiguration of the agents is required. Every time that an agent is reached by the robot,it is consumed and a new one, that becomes the new explorer is added to the end of the curve toward the final goal. In Fig. 3.9 it is shown an example of the reconfiguration mechanism. The masses of the agents are scaled accordingly.

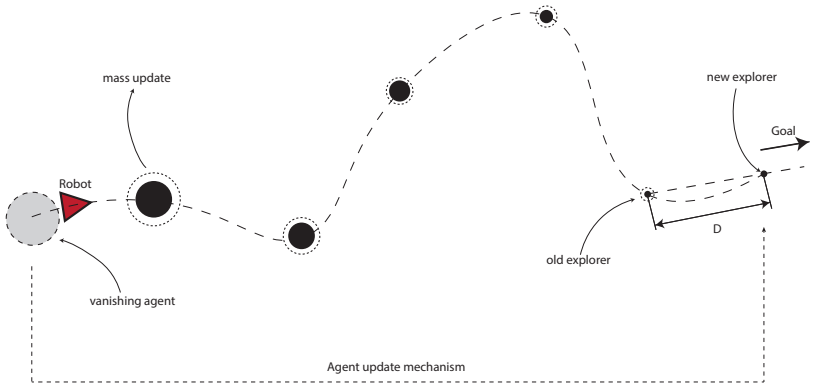

FIGURE 3.9: Agent reconfiguration

The overall behaviour of the algorithm can be described as follows:

Algorithm 1 Pac-Man algorithm

```
1: procedure REACH_GOAL
2:     trajectory ← create_trajectory_toward_goal(number_of_agents)
3:     while goal_not_reached do
4:         move_robot_to_next_point(trajectory)
5:         if next_agent_reached then
6:             remove_previous_agent(trajectory)
7:             add_new_agent_toward_goal(trajectory)
8:         update(trajectory)
```

3.6 Experimental results

The experimental tests for the proposed path planner have been tested in a purposedly built arena characterized by a $3x3m$ area in which several obstacle have been randomly placed. A system of Vicon cameras (Vicon, Oxford, UK), working at their maximum frequency (250 fps) has been employed to track the position in time of both the obstacles and the Kuka YouBot mobile platform chosen for the tests. Each experiment consisted in making the robot reach the opposite side of the arena while avoiding collision with the environment. In Fig. 3.10 five snapshot of one of the 50 tests performed are proposed to give an idea of the working patterns of the algorithm. The reconstruction of the arena in Rviz, the ROS visualization tool, has

FIGURE 3.10: Snapshots of robot motion and Rviz interface.

been superimposed on real images to furtherly improve the understanding of the via point dynamics.

It is then possible to see the agents' interaction with the potential environment (the light brown coloured regions around the cylinders modelling the obstacles) that leads to the definition of a smooth curve guiding the robot along the fastest path to the final goal.

The parameters chosen for the proposed tests are proposed in Table 3.1

In the sequence of figures it is possible to appreciate how the exploring agents interact with the potential field generated by the obstacles and modify their position accordingly, producing a smooth trajectory that circumnavigates the area around the obstacles. The convoying agents providing the instantaneous references for the motion are unaffected by the modification of the trajectory caused by the explorers. As result an overall trajectory characterized by a constant velocity along the defined path is generated. In the tests performed over fifty different scenarios, characterized by obstacles randomly generated but whose potential fields are not interacting with each other, the success rate has been of 100%. Moreover the generation of the initial

TABLE 3.1

Variable	Value	Unit	Variable	Value	Unit
δ_r	0.1	[m]	ϕ_b	0.35	[Nm]
k	1	[N/m]	g_0	-1	[N]
n	15		ρ	0.25	[m]

trajectory by means of a sample-based planner has allowed to extend the result to environments in which the interaction between the potential fields is considered. The analysis of the generated trajectory showed that, by taking into account the parameters values defined in 3.1, the agents become stable in 1.25 seconds, on average. This result confirms the reactiveness of the algorithm with respect to dynamical changes in the environment and its low computational burden.

3.7 Conclusion

A new planning technique, that exploits the properties of Uniform B-spline curves and FIR filters, has been proposed and evaluated through a series of experimental test with a kuka youBot mobile platform. The via points of the B-spline have been characterized as dynamic mass-spring-damper systems that interact with the environment and provide a real time reacting trajectory for the mobile base. The result here obtained, validated by the experimental tests can be easily applied in a teleoperation scenario, in which the operator can directly impose the direction of motion, i.e. the current target of the explorer, while the system automatically takes care of the surrounding scenario. This becomes very interesting in presence of the control of a mobile base when the user is focused on a manipulation task as will be discussed in the next chapter. It can also prove very effective as safety in the control of the robotic arm in presence of human being or other robotic manipulators, where the system could automatically provide modifications to the commanded trajectory to avoid danger to surrounding elements. The result of this word has been presented at the 12th IFAC Symposium on Robot Control (SYROCO 2018) [78].

Chapter 4

A new mapping technique for task-centered teleoperation

4.1 Haptic control of mobile manipulators

The teleoperation of mobile manipulators pose interesting challenge since the control of two very different structural systems, a mobile base and a robotic arm, must be considered.

FIGURE 4.1: A Tiago mobile manipulator from Pal Robotics

As discussed in the chapter 1 the control schemes for a robotic arm and a mobile base can be quite different. The task of unifying the two kind of approaches in a comprehensive and intuitive way for the human operator is still an open reserach subject. Nevertheless several solutions that try to define new hybrid control paradigms have already been proposed [79] [80] [81] [82]. The considered solutions usually implement several operation modes according to the present situation to be handled. In each operation modes a different mapping technique for both the base and the arms is applied. Three main families of algorithm can be defined according to the implementation of the switching mode [79]:

- **Manual methods**: the operation mode is modified by a mechanical switch on the master side. Additional hardware must be present for this kind of solution. A simple example consider the switch between a position control of the arm and the motion control of the mobile base. A more complex solution involve

the use of a redundant differential inverse kinematic to solve the control problem in locomotion mode (motion in free space) with respect to the control of the robotic arm only in position mode (motion in unstructured environment) [80];

- **Manual-automatic methods**: The switch between the control modes is done according to predefined map of the environment. The robot switchs to the position control of the arm when close to fixed working areas in the workspace. The proposed switching rule is described by:

$$\text{strategy} = \begin{cases} \text{position-speed} & \text{if } d > d_c \\ \text{position-position} & \text{if } d \leq d_c \end{cases} \tag{4.1}$$

where d represents the slave distance to the region of interest and d_c the distance at which the switch should take place. This kind of strategies requires a good knowledge of the working environment and it presents low flexibility to unknown situations or modifications;

- **Automatic methods**: the control strategy is automatically chosen by the system according to the velocity of the user motion and to the presence of any obstacle near the slave device. The automatic switching rule is defined by:

$$\text{strategy} : \begin{cases} \text{position-speed} & \text{if } \dot{X}_h > v_h \text{ and } d > d_c \\ \text{position-position} & \text{if } \dot{X}_h \leq v_h \text{ or } d \leq d_c \end{cases} \tag{4.2}$$

where v_h is the velocity threshold, L is the distance from the nearest obstacle and L_c is the minimum safety distance from the obstacle.

A different typology of algorithms focus on merging the different control modes aiming at removing the delays imposed by the switch and the consequent reconfiguration of the mapping. The idea is to partition the control space of the devices so that the control algorithms can coexist and eventually work concurrently. This choice, although it could potentially cause a reduction in the dimension of the control workspace in each control mode, should allow the simplification of the task for the human operator, that is allowed to focus on the task at hand without the need to consider required changes in the control scheme due to environment conditions. It is then possible to define a different characterization of the mapping algorithms [82]:

- **Manual strategy**: the switching between the control modes is done manually by the user, no merging applied;
- **Master workspace strategy**: the operational mode is changed according to the pose of the master handle. The workspace of the master device is partitioned in two or more working areas to which a different control mode is assigned.
- **Slave workspace strategy**: the operational mode is changed according to the slave end effector position with respect to its base reference frame.

All the proposed solution are balancing a trade-off between intuitivity, task precision and performance: manual control mode guarantee the use of the full dimension of

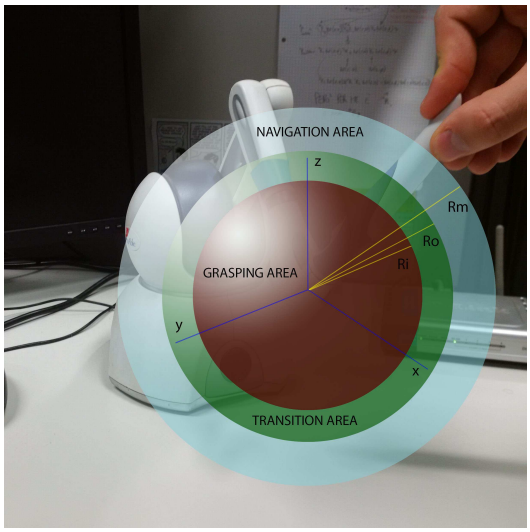

FIGURE 4.2: Workspace characterization

the workspace of the master device for the control task but requires the operator to focus on the choice of the mode and have increased overheads due to reconfiguration; on the other hand hybrid strategies provide more intuitivity and performance to the operator at the cost of a reduction of the control workspace.

4.2 A new hybrid control scheme

The new solution proposed in this work considers a master workspace strategy that allows the human operator to abstract himself from the different behaviours of the low level controls of the components of the mobile manipulator with the purpose of focusing only on the task at hand. The idea is to provide a shared control framework in which the attention of the user can be kept on the motion of the end-effector while the robotic system takes care of the various subsystems. This has been obtained by defining different control areas inside the master workspace as shown in Fig. 4.2.

Inside the haptic workspace three concentrical regions are identified. Their center is defined as the center of the sphere of maximum radius inscribed in the whole workspace. The radius R_m of the inscribed sphere defines the maximum spatial extension of the partitioned workspace. The two inner spherical surfaces of radius R_i and $R_o = R_i + \epsilon$ partition the master workspace in three different areas, the grasping area, the navigation area and the transition area. The three regions defined this way are characterized as follows:

- **The grasping area**: is the area comprised inside the spherical region of radius R_i. It is the area assigned to the control of the robotic manipulator only, in which the mobile base is kept still. While working in this area the manipulator is considered capable of reaching and interacting with all the object of interest without the assistance of the base;

- **The navigation area**: is the area defined between the spherical regions of radius R_o and R_m. It is the most external area of the master workspace and is assigned to the control of the mobile base. This area is reached by the user

when the task objective is placed beyond the current manipulator limits and thus the assistance of the mobile base to reduce the distance is required.

- **The transition area**: is the area of transition between the previously defined control laws. It is used to achieve a smooth transition between the control systems in such a way that the external operator do not sense a discontinuity in the end-effector motion.

While the external radius R_m is strongly related to the physical characteristics of the haptic device, the dimenntions of the internal regions can be designed according to the task at hand. In the following some specific details on the three control regions will be addressed.

4.2.1 Grasping Area

In this region a standard position control scheme, as already described in Chapter 1, has been chosen, see (1.13). The scaling factor k is tuned in such a way that the whole workspace of the slave arm can be directly controlled. Given R_s the smallest spherical surface inscribed in the workspace of the slave arm, the factor is obtained by:

$$k = \frac{1}{R_o / R_s} = \frac{R_s}{R_o} \tag{4.3}$$

Depending on the value of R_s, it is then possible to choose the parameter R_o $(< R_m)$ so that scale factor of the scheme allows a proper resolution for the manipulation task to be completed.

4.2.2 Navigation Area

The outer navigation area can be only reached by forcing a temporary expansion of the inner sphere through the application of a force against its surface, that modifies its radius R_o according to the user movements. The end-point is subject to an elastic force, proportional to the expansion of R_o, that tries to restore the original dimension of the region. During the expansion the scale factor of the position control of the arm is modified in such a way that the position reference for the arm keeps a constant value. This way inside the navigation area the controlled arm modifies only its orientation and any position mismatch when the control is returned inside the grasping area is prevented. The velocity control in the two external regions is characterized by a standard rate control scheme (see (1.14)). The scale factor k is chosen so that the maximum velocity for the base is achieved at the limit of the external workspace:

$$k = \frac{V_{max}}{R_m - R_i} \tag{4.4}$$

The constant factor k, used to map the whole velocity range of the mobile platform, is obtained according to the choice of R_o during the design phase. The feedback response is characterized by an elastic behaviour proportional to the expansion induced to the sphere as already presented in Chapter 1. Fig. 4.3 shows the velocity direction mapping for the mobile base. In case of an holonomic base is considered the reference is commanded with respect to the center of the mobile base. Rotation is accomplished by considering also the z axis of the master device.

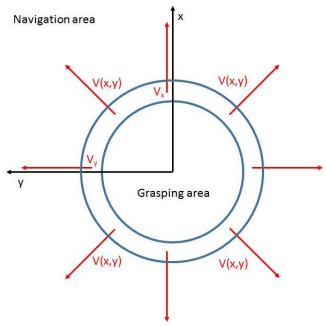

FIGURE 4.3: Velocity generation

4.2.3 Transition Area

The transition area guarantees a smooth switch between the arm and the base motion: while the master end-point is crossing the region the mobile base starts to increase its velocity, while the arm progressively reduces its speed until it stops when the final position is reached. This reduction is obtained by defining a third order polynomial function in the mapping between the master and slave arm positions, as shown in Fig. 4.4 (green line).
The chosen polynomial trajectory is evaluated with the following parameters:

$$q_i = \frac{R_i R_o}{R_s}, \quad q_f = \frac{R_s(R_o - R_i)}{2R_o} + q_i$$

$$q_{v_i} = \frac{R_s}{R_o}, \qquad q_{v_f} = 0$$

The choice as final position of the central point between the boundary of slave workspace and the radius R_i allows the prevent singularity situations from arise. Given its definition as function of R_i, q_i can be seen as a trade off between the percentage of slave workspace covered and the considered distance from singularity configurations. The final mapping in the transition area is described by:

$$X_s = -0.5\frac{R_s}{R_o^2 - R_o R_i}(p_m - R_i)^2 + \\ + \frac{R_s}{R_o}(p_m - R_i) + \frac{R_s R_i}{R_o}$$

The overall behaviour of the slave robotic arm with the master moving through the three working areas is shown in Fig. 4.4

4.3 An improved mapping control

The proposed control scheme, presented at Intelligent Robots and Systems (IROS 2016) [83], still suffers from some concerning issues:

- The trade-off in the definition of the spherical regions imposes a significant limit to the precision of the manipulation task.
- The algorithms, as the other hybrid algorithms for mobile manipulators, suffers from the arm position during the motion of the base: since the switch

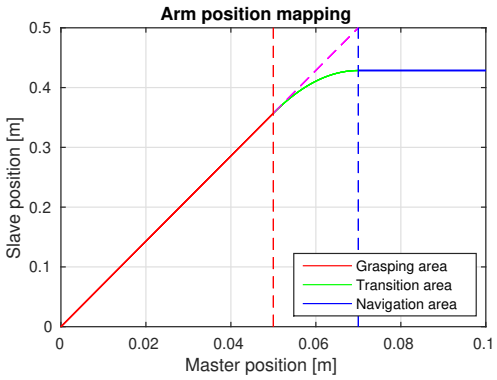

FIGURE 4.4: Mapping between the master and slave arm positions.

between the operation modes is performed when the arm is near the border of its workspace the manipulator is forced to move in the environment with an extended arm or suffers from additional pairing time when the system is returned to the manipulation mode.

- The definition of the control regions as proposed above do not fully exploit the capabilities of the master workspace.

The analysis of these problems has led to the definition of an improved version of the proposed control that focus on two aspects:

- The dimension of the master workspace in each control mode;
- The level of flexibility given by the definition of the control regions.

4.3.1 A mobile system

The definition of spherical control regions in the master workspace allows to map a motion for the arm that covers almost its whole workspace, that is usually characterized by a spherical space centered in the manipulator's base link reference frame. The addition of a mobile base to the system allows to exploit the base motion in the planning of the pick pose for the robot, therefore several poses in the arm workspace are no longer required to be mapped since an equivalent motion can be obtained by reorienting the robot itself. It is then sufficient to consider for the arm only the frontal semi-spherical region. Because of this it has been possible as well to consider a semi-spherical region covering all the master workspace by adding an offset along the x direction in such a way to define the center of the spherical areas at the physical limit of the device along x and by expanding accordingly the radius of the control areas. This choice in the workspace definition has allowed to double the dimension of the regions themselves, thus halving the scale factor for the control of the arm.

4.3.2 A dynamical border

Besides the obvious advantage produced by the change of the geometry of the master workspace, the mapping is still affected by the trade-off between the control space assigned to the mobile base and the robotic arm. An optimal solution for both the control scheme would require the full workspace to be assigned to a single

mapping when the other control mode is not required. This could be easily obtained by using a mechanical switch, if present on the haptic device, to change the control mode as already exploited by several of the algorithm presented at the beginning of this chapter. On the other hand this solution would require a direct intervention of the human operator in the change of control mode, that would lead to a reduction in the abstraction level that the system could provide. In fact the operator could no be any more uniquely focused on the task performed with the manipulator end effector but would also need to take care of the changes of control scheme, therefore taking into consideration the mobile manipulator as two different subsystems instead of a whole one. A more challenging approach lies then in trying to achieve the same result (full workspace for both controls) while keeping the switch procedure automatic. This can be achieved by considering a variable radius for the internal regions previously defined. The new mapping proposed will be characterized as follows:

- When the master is controlled inside the inner region and only the arm is in motion the value of the radius R_i and R_o are brought to R_{max}, close to R_m, defining a control region for the arm that covers nearly all the master workspace;
- When the master handle is moved in the transition area the value of R_i and R_o is reduced to avalue R_{min} close to the center of the haptic reference, defining a control region for the mobile base that covers again nearly all the master workspace;
- When the master handle is returned to the inner region the radius are increased again.

This change of the dimension of the control areas during the task allows to fully exploit the master workspace. In addition the reduction of the grasping area during the base motion causes the robotic manipulator to be retracted toward the robot torso, both reducing the risk for unexpected collision and simplifying the operator task to plan the robot movements. The final behaviour of the control mapping is highly influenced by the dynamic of the two inner radius. In order to define the most intuitive control for the operator several different transient dynamics, both during during the expansion and the reduction of the control regions, have been considered. In the following the definition of the different transition dynamic will be proposed considering only the inner radius R_i and the expansion case. This :

- **Static transition**: the value of the radius is not modified:

$$R_i = R_0 \tag{4.5}$$

  where R_0 is the radius initial value. This control corresponds to the original control technique;

- **Step transition**: the value of the radius is immediately changed to the final value:

$$R_i = R_{max}. \tag{4.6}$$

- **Linear transition**: the value of the radius is continuously increased in each control cycle up to the final value, the incremental rate is constant:

$$R_i = R_i + d \text{ if } R_i < R_{max} \tag{4.7}$$

where d is the radius increase in each cycle;

- **Incremental transition**: the value of the radius is increased in each control cycle up to the final value, the incremental rate is linear in time:

$$R_i = R_i + d \text{ if } R_i < R_{max} \tag{4.8}$$
$$d = d + d_g \tag{4.9}$$

with d_g the incremental factor.

- **Controlled transition**: the value of the radius is increased in each control cycle up to the final value, the incremental rate is linear in time and its initial value d_0 is proportional to the force F_h applied to the bubble by the operator:

$$R_i = R_i + d \text{ if } R_i < R_{max} \tag{4.10}$$
$$d = d + d_g \tag{4.11}$$
$$d_0 = kF_m \tag{4.12}$$

The reduction transients can be controlled in the same way. The radius R_o can be obtained as function of R_i as explained in section 4.2. The different characteristics and performance of the proposed transient behaviours will be tested and confronted in the second part of the experimental tests.

4.4 Experimental tests

The experimental test have been carried out on two different robotic platforms according to the scheme proposed in Fig. 4.5.

A Geomagic Phantom Omni Haptic device has been used as master device. The

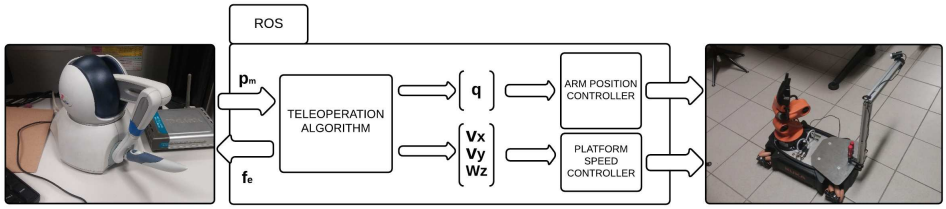

FIGURE 4.5: System used for the experimental evaluation.

Phantom Omni is characterized by 6 degree of freedom robotic arm equipped with a removable stylus and two physical switchs. It is equipped with position encoder on all the joint axes and with three motors providing force feedback along the three main axis in the first three joints. The position of the haptic stylus in the operational space is obtained by the measured values of the joints through a predefined homogeneous transform. The kuka youbot and the Pal Tiago have been chosen as slave devices. The kuka youbot is characterized by an holonomic base equipped with four sweedish wheels and two 5 dof robotic arms. An internal computer running Ubuntu 14.04 allows the control of the low level systems and acts as a intermediate layer with the network. The Pal Tiago is characterized by a non-holonomic base and a 7 dof arm mounted on a liftable torso. The internal computer allows the control of all the subsystems and provide some high level framework for the access to the

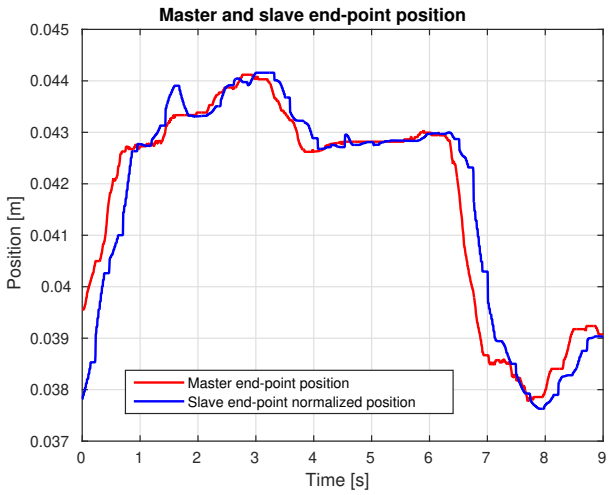

FIGURE 4.6: Master and slave position tracking along x.

robot functions. All the software has been developed in the Robotic Operating System (ROS). The first results discussed here, measured with the YouBot platform, are related to a generic grasping task characterized by two phases: at the beginning the slave robot is used to grasp an object within its workspace, then it is asked to bring the object to a point far from it, required the use of all the operational modes.

Three specific aspects will be studied and discussed:

- The control of the robotic arm in manipulation mode;
- The response obtained by the transition mapping;
- The overall behaviour of the system while moving between the different control regions.

Following the general procedure described in section 2, the final parameter for the YouBot system are:

$$R_m = 0.1 \quad [m] \tag{4.13}$$
$$R_s = 0.5 \quad [m] \tag{4.14}$$
$$R_o = 0.07 \quad [m] \tag{4.15}$$
$$k = 7.14 \tag{4.16}$$
$$R_i = 0.05 \quad [m] \tag{4.17}$$
$$V_{max} = 0.8 \quad [m/s] \tag{4.18}$$

The value $k = 7.14$ represents a good trade-off between the necessity of a good accuracy and an equal spatial division between the regions.

Fig. 4.6 shows the performance of the master slave system in a grasping task performed in pure manipulation mode. The slave signal in the figure has been normalized by a scale factor to allow a proper comparison. IT is possible to appreciate the successful tracking of the master position despite the presence of a time delay of 0.2 s that can be imputed to the expected delay in the ROS network.

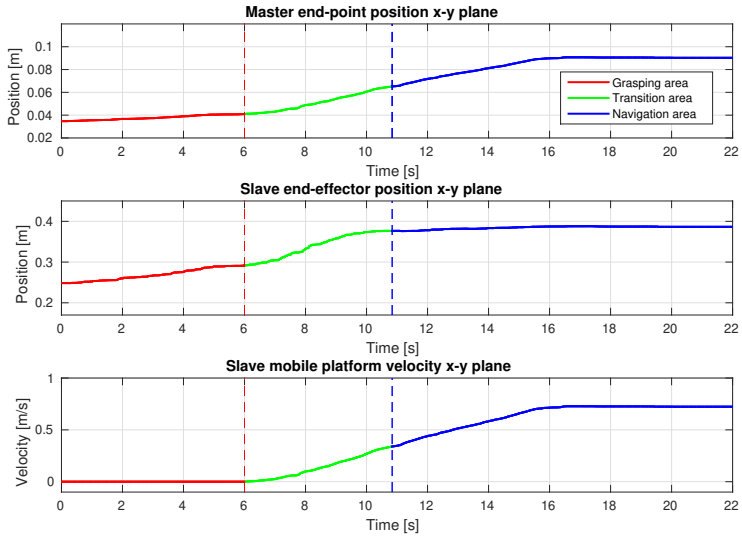

FIGURE 4.7: Master and slave position (projection of p_s in the $x-y$ plane) and mobile platform velocity through the three control regions.

4.4.1 Master/Slave position mapping in the transition area

Figure 4.8 shows the position mapping between the master and the slave device during the transition phase between the grasping and the navigation area.

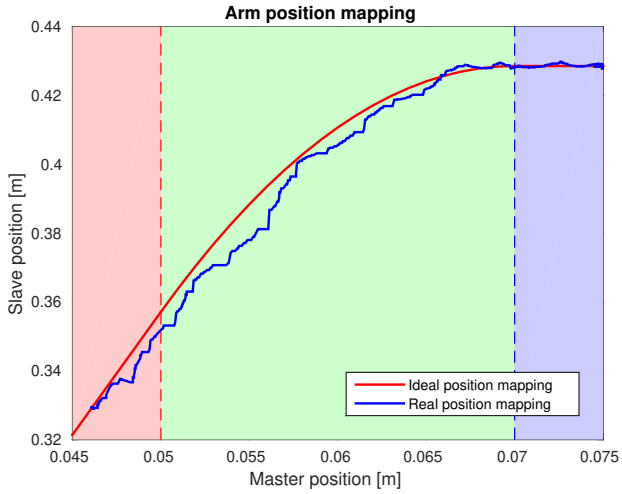

FIGURE 4.8: Master and slave mapping across the transition area. Red area: grasping; green area: transition; blue area: navigation.

The red curve in the graph represents the ideal trajectory generated by the control scheme, while the blue one is obtained from the data measurements. It can be seen that a satisfactory tracking of the desired reference is achieved by the system: the final position reached by the arm is the desired value (far away from singular configurations).

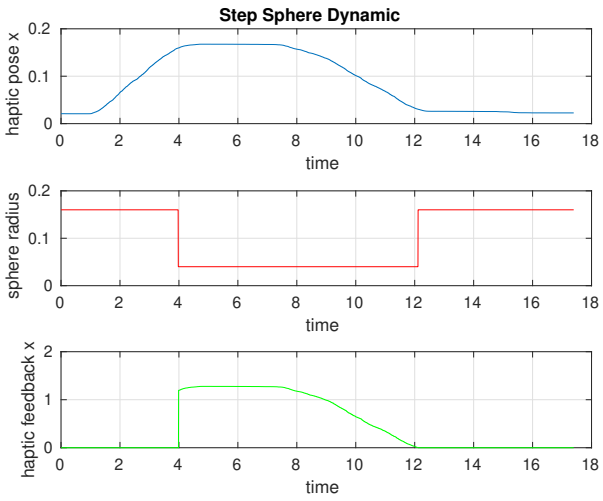

FIGURE 4.9: Step dynamic of the radius of the internal region and overall force feedback produced by the motion along x of the master device.

4.4.2 Improved mapping tests

The tests on the different dynamic for the radius of the grasping area have considered in particular the crossing motion between the two regions for the control of the arm and of the base. The modifications to the algorithm required a different tuning of some of the parameters as follows:

$$R_m = 0.2 \quad [m] \tag{4.19}$$

$$x_w = -0.1 \quad [m] \quad R_{i_{min}} = 0.04 \quad [m] \tag{4.20}$$

$$R_{i_{max}} = 0.16 \quad [m] \tag{4.21}$$

$$\tag{4.22}$$

where the last two parameters represent the minimum and maximum value for the radius R_i, whose initial value has been set to R_{i_max} since the manipulation always starts inside the grasping area. The results proposed here will show the modification of the sphere radius R_i and the force feedback generated by the navigation area control according to the different dynamic choices. A slow motion along the x axis of the master has been pre-recorded and used as reference for the three tests. The first one has considered a step dynamic transition as shown in Fig. 4.9.

Once the haptic device enters the transition area ($|X_h| > R_i$) the radius of the sphere is immediately reduced to the minimum R_{i_min}, therefore inducing an high force feedback on the operator and an elevated acceleration on the mobile base. When the master handle is progressively brought back near the origin, an equivalent reduction can be observed in the feedback force. As the haptic device returns in the grasping area ($|X_h| < R_i$) the initial value of the radius is immediately restored. This choice for the dynamic provides immediately the full workspace both during the work in the grasping and the navigation area and proves particularly intuitive from the operator point of view. On the other sides in particular working conditions presents some drawbacks:

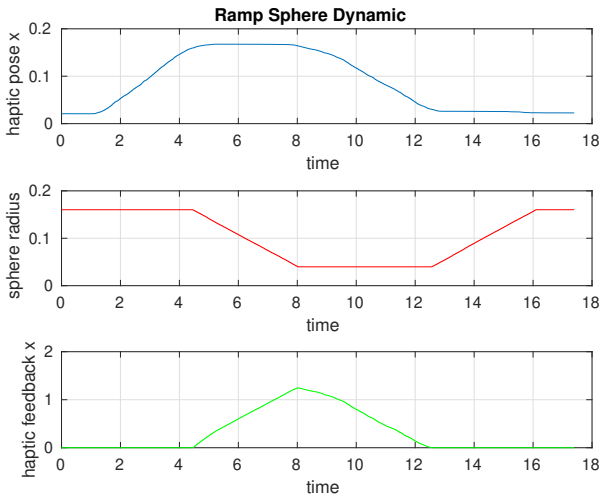

FIGURE 4.10: Ramp dynamic of the radius of the internal region and overall force feedback produced by the motion along x of the master device.

- When the operator enters the transition area a step feedback can be perceived by the operator, directly influencing its movements;
- When just several quick and slow motions for the base are required, the operator is still forced to every time to move through the whole master workspace any time a switch is required, resulting in additional overheads and unnecessary motions of the arm.

A gentler behaviour can be observed when a ramp dynamic is applied to the radius, see Fig. 4.10.

The radius decreases or increases linearly on each control cycle. This type of dynamic acts as a trade-off between the static and the step case: a big value of the incremental parameter d would determine a rapid convergence to the final value, producing a similar dynamic to the step case whereas a low value would require in many cases for the operator to wait for the expansion or reduction to be completed before proceeding with the control. Eventually a more interesting behaviour can be observed in the incremental or the controlled case, see Fig. 4.11. Two different behaviour can be observed during the incremental modification:

- Immediately after the switch the incremental rate is quite low and the modifications to the control areas are not noticeable to the human operator; this becomes particularly useful when many fast switches, usually derived by small adjustments in the end effector pose, are required.
- When the incremental factor has grown enough the change in radius becomes much more important and the region rapidly converges to its steady state configuration.

Despite its advantages this choice for the dynamic still presents a disadvantage when a constant slow motion of the base is required for a long time. In this scenario the movement required for the switch would still be noticeable to the operator

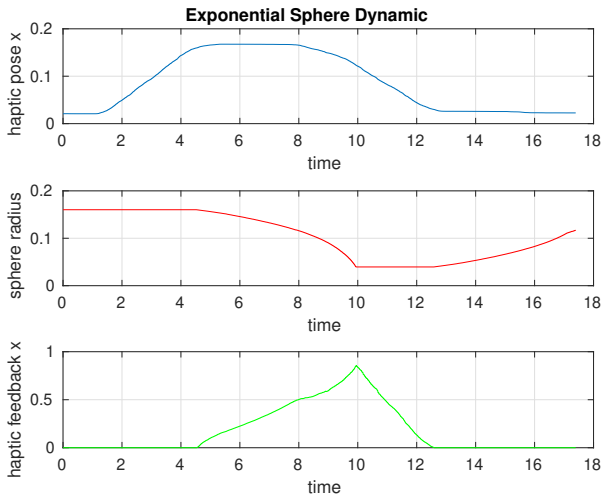

FIGURE 4.11: Incremental dynamic of the radius of the internal region and overall force feedback produced by the motion along x of the master device.

because of the overall small deceleration required to stop the base motion, overextended by the radius reduction. This problem is solved with the controlled dynamic, since the modification of the incremental rate is defined according to the level of velocity imposed to the base: for slow base motion the incremental rate is kept within small values and the control regions result modified only after a consistent period of time while on the other hand fast base motion impose quick changes to increase the manoeuvrability of the system. The controlled dynamic of the radius results then the best solution among the proposed ones for the dynamic reduction of the grasping area. Different considerations have instead to be taken concerning the expansion phase. In fact since the velocity of the robot reaches zero when the system switchs back into the grasping area a natural prosecution of the motion would concern exclusively the robotic arm. Because of this many switches between the regions are not likely to happen and the immediate availability of the widest regions for the control of the arm is preferable. The step dynamic proves than the best approach for the expansion dynamic.

4.5 Conclusions

In this chapter a new control mapping technique for the control of a mobile manipulator by means of a single commercial haptic device has been presented. The new control is characterized by the division of the workspace of the master in different control areas of variable dimension in time, according to the user motion. The partition of the workspace allows to control both the base and the arm from the same motion, supporting a more task-centered control for the operator. The first part of this work was presented at Intelligent Robots and Systems (IROS 2016) [83] . The next part of the study will concern the evaluation of a grasping task in an unstructured environment performed by a batch of non trained users and the implementation of the bilateral force feedback for the arm according to the schemes proposed in

Chapter 1. This will allows to obtain additional proofs of the validity of the control scheme and will also expose any remaining weakness to be addressed.

Chapter 5

Conclusions

In this work three different aspects of the haptic control of mobile manipulator and their interaction with the environment have been addressed. At first the dynamic of object manipulation vibration, in particular in operations where liquid containers are moved has been studied. A feed-forward plug-in method characterized by an online filtering of the operator trajectory plus a proper reorientation of the controller container has been developed and tested. Then a second study concerning trajectory planning with real-time obstacle avoidance for mobile base or arm motion has been carried out. The analysis of B-spline trajectories has allowed to define a new planner based on the via-point of the trajectory, characterized as virtual mass-spring-damper systems interacting with the environment. Eventually the problem of simplifying the haptic control of a mobile manipulator for the human operator has been considered. A new mapping technique, that could allows the operator to focus on the task at hand while the mobile manipulator is automatically controlling the low level subsistems, has been proposed. The experimental tests have confirmed the validity of the work. Particular attention has been brought toward the operator, keeping in mind a framework in which its task was made as intuitive as possible while at the same time he was mantaining direct control of the system. The three algorithms can be considered as the first part of a larger study to reach a complete integrated control scheme for haptic manipulation of the mobile manipulators interacting with the environment. The next part of the work will be characterized by:

- The development of the vision system
- The development of a learning network able to learn and predict the operator goal to provide additional assistance via haptic feedback
- The development of an assistive pick pose detector to simplify the grasp task
- The improvement of the slosh removal filter for the mobile manipulator case

The final step of the work will concern the integration of all the algorithms under a unified control scheme and the performance of the final tests for the system.

Bibliography

[1] Thomas B Sheridan. "Space teleoperation through time delay: Review and prognosis". In: *IEEE Transactions on robotics and Automation* 9.5 (1993), pp. 592–606.

[2] Peter F Hokayem and Mark W Spong. "Bilateral teleoperation: An historical survey". In: *Automatica* 42.12 (2006), pp. 2035–2057.

[3] S Lichiardopol. "A survey on teleoperation". In: *Technische Universitat Eindhoven, DCT report* (2007).

[4] Riccardo Muradore and Paolo Fiorini. "A review of bilateral teleoperation algorithms". In: *Acta Polytechnica Hungarica* 13.1 (2016), pp. 191–208.

[5] Forrest T Buzan and Thomas B Sheridan. "A model-based predictive operator aid for telemanipulators with time delay". In: *Systems, Man and Cybernetics, 1989. Conference Proceedings., IEEE International Conference on*. IEEE. 1989, pp. 138–143.

[6] Blake Hannaford. "A design framework for teleoperators with kinesthetic feedback". In: *IEEE transactions on Robotics and Automation* 5.4 (1989), pp. 426–434.

[7] Blake Hannaford. "Stability and performance tradeoffs in bi-lateral telemanipulation". In: *Robotics and Automation, 1989. Proceedings., 1989 IEEE International Conference on*. IEEE. 1989, pp. 1764–1767.

[8] Blake Hannaford and Paolo Fiorini. "Detailed model of bi-lateral teleoperation". In: *Proceedings of the 1988 IEEE International Conference on Systems, Man, and Cybernetics*. 1988.

[9] Dale A Lawrence. "Stability and transparency in bilateral teleoperation". In: *IEEE transactions on robotics and automation* 9.5 (1993), pp. 624–637.

[10] Robert J Anderson and Mark W Spong. "Bilateral control of teleoperators with time delay". In: *IEEE Transactions on Automatic control* 34.5 (1989), pp. 494–501.

[11] Günter Niemeyer and J-JE Slotine. "Stable adaptive teleoperation". In: *IEEE Journal of oceanic engineering* 16.1 (1991), pp. 152–162.

[12] Dongjun Lee and Ke Huang. "Passive-set-position-modulation framework for interactive robotic systems". In: *IEEE Transactions on Robotics* 26.2 (2010), pp. 354–369.

[13] Blake Hannaford and Jee-Hwan Ryu. "Time-domain passivity control of haptic interfaces". In: *IEEE Transactions on Robotics and Automation* 18.1 (2002), pp. 1–10.

[14] Michel Franken et al. "Bilateral telemanipulation with time delays: A two-layer approach combining passivity and transparency". In: *IEEE transactions on robotics* 27.4 (2011), pp. 741–756.

[15] Cristian Secchi, Federica Ferraguti, and Cesare Fantuzzi. "Catching the wave: A transparency oriented wave based teleoperation architecture". In: *Robotics and Automation (ICRA), 2016 IEEE International Conference on*. IEEE. 2016, pp. 2422–2427.

[16] Federica Ferraguti, Cesare Fantuzzi, and Cristian Secchi. "Optimizing the use of power in wave based bilateral teleoperation". In: *Intelligent Robots and Systems (IROS), 2016 IEEE/RSJ International Conference on*. IEEE. 2016, pp. 1469–1474.

[17] Jeroen GW Wildenbeest et al. "The impact of haptic feedback quality on the performance of teleoperated assembly tasks". In: *IEEE Transactions on Haptics* 6.2 (2013), pp. 242–252.

[18] Oussama Khatib et al. "Spanning large workspaces using small haptic devices". In: *null*. IEEE. 2005, pp. 183–188.

[19] P Chotiprayanakul and DK Liu. "Workspace mapping and force control for small haptic device based robot teleoperation". In: *Information and Automation, 2009. ICIA'09. International Conference on*. IEEE. 2009, pp. 1613–1618.

[20] Mohamed Mamdouh and Ahmed A Ramadan. "Development of a teleoperation system with a new workspace spanning technique". In: *Robotics and Biomimetics (ROBIO), 2012 IEEE International Conference on*. IEEE. 2012, pp. 1570–1575.

[21] Alaa Khalifa et al. "Workspace mapping and control of a teleoperated endoscopic surgical robot". In: *Methods and Models in Automation and Robotics (MMAR), 2014 19th International Conference On*. IEEE. 2014, pp. 675–680.

[22] Nicola Diolaiti and Claudio Melchiorri. "Teleoperation of a mobile robot through haptic feedback". In: *Haptic Virtual Environments and Their Applications, IEEE International Workshop 2002 HAVE*. IEEE. 2002, pp. 67–72.

[23] Donald A Norman. "The âĂŸproblemâĂŹwith automation: inappropriate feedback and interaction, not âĂŸover-automationâĂŹ". In: *Phil. Trans. R. Soc. Lond. B* 327.1241 (1990), pp. 585–593.

[24] Charles E Billings. *Aviation automation: The search for a human-centered approach*. CRC Press, 2018.

[25] Raja Parasuraman and Christopher D Wickens. "Humans: Still vital after all these years of automation". In: *Human factors* 50.3 (2008), pp. 511–520.

[26] David A Abbink and Mark Mulder. "Neuromuscular analysis as a guideline in designing shared control". In: *Advances in haptics*. InTech, 2010.

[27] Thomas B Sheridan. *Telerobotics, automation, and human supervisory control*. MIT press, 1992.

[28] Frank Flemisch et al. "Automation spectrum, inner/outer compatibility and other potentially useful human factors concepts for assistance and automation". In: *Human Factors for assistance and automation* 2008 (2008), pp. 1–16.

[29] Christopher A Miller and Raja Parasuraman. "Designing for flexible interaction between humans and automation: Delegation interfaces for supervisory control". In: *Human factors* 49.1 (2007), pp. 57–75.

[30] David A Abbink. "Neuromuscular analysis of haptic gas pedal feedback during car following". In: (2006).

[31] S De Stigter, Max Mulder, and MM Van Paassen. "Design and evaluation of a haptic flight director". In: *Journal of guidance, control, and dynamics* 30.1 (2007), pp. 35–46.

[32] Mark Mulder, David A Abbink, and Erwin R Boer. "The effect of haptic guidance on curve negotiation behavior of young, experienced drivers". In: *Systems, Man and Cybernetics, 2008. SMC 2008. IEEE International Conference on*. IEEE. 2008, pp. 804–809.

[33] DA Abbink and M Mulder. "Exploring the dimensions of haptic feedback support in manual control". In: *Journal of Computing and Information Science in Engineering* 9.1 (2009), p. 011006.

[34] Thanh Mung Lam et al. "Artificial force field for haptic feedback in UAV teleoperation". In: *IEEE Transactions on Systems, Man, and Cybernetics-Part A: Systems and Humans* 39.6 (2009), pp. 1316–1330.

[35] Marcia K OâĂŹMalley et al. "Shared control in haptic systems for performance enhancement and training". In: *Journal of Dynamic Systems, Measurement, and Control* 128.1 (2006), pp. 75–85.

[36] Louis B Rosenberg. "Virtual fixtures: Perceptual tools for telerobotic manipulation". In: *Virtual Reality Annual International Symposium, 1993., 1993 IEEE*. IEEE. 1993, pp. 76–82.

[37] Panadda Marayong and Allison M Okamura. "Speed-accuracy characteristics of human-machine cooperative manipulation using virtual fixtures with variable admittance". In: *Human Factors* 46.3 (2004), pp. 518–532.

[38] David A Abbink, Mark Mulder, and Erwin R Boer. "Haptic shared control: smoothly shifting control authority?" In: *Cognition, Technology & Work* 14.1 (2012), pp. 19–28.

[39] Paul G Griffiths and R Brent Gillespie. "Sharing control between humans and automation using haptic interface: primary and secondary task performance benefits". In: *Human factors* 47.3 (2005), pp. 574–590.

[40] Benjamin AC Forsyth and Karon E MacLean. "Predictive haptic guidance: Intelligent user assistance for the control of dynamic tasks". In: *IEEE transactions on visualization and computer graphics* 12.1 (2006), pp. 103–113.

[41] Kenneth H Goodrich et al. "Application of the H-mode, a design and interaction concept for highly automated vehicles, to aircraft". In: *25th Digital Avionics Systems Conference, 2006 IEEE/AIAA*. IEEE. 2006, pp. 1–13.

[42] Vitalii Pruks, Kwang-Hyun Lee, and Jee-Hwan Ryu. "Shared Teleoperation for Nuclear Plant Robotics Using Interactive Virtual Guidance Generation and Shared Autonomy Approaches". In: *2018 15th International Conference on Ubiquitous Robots (UR)*. IEEE. 2018, pp. 91–95.

[43] Shervin Javdani et al. "Shared autonomy via hindsight optimization for teleoperation and teaming". In: *The International Journal of Robotics Research* (2018), p. 0278364918776060.

[44] Anca D Dragan and Siddhartha S Srinivasa. "A policy-blending formalism for shared control". In: *The International Journal of Robotics Research* 32.7 (2013), pp. 790–805.

[45] Pete Trautman. "Assistive planning in complex, dynamic environments: a probabilistic approach". In: *Systems, Man, and Cybernetics (SMC), 2015 IEEE International Conference on*. IEEE. 2015, pp. 3072–3078.

[46] Luigi Biagiotti et al. "A plug-in feed-forward control for sloshing suppression in robotic teleoperation tasks". In: *Intelligent Robots and Systems (IROS), 2018 IEEE/RSJ International Conference on*. IEEE. 2016.

[47] K. Terashima, M. Hamaguchi, and K. Yamaura. "Modelling and input shaping control of liquid vibration for an automatic pouring system". In: *Decision and Control, 1996., Proceedings of the 35th IEEE Conference on*. Vol. 4. 1996, pp. 4844–4850.

[48] Ameen Aboel-Hassan, Mustafa Arafa, and Ashraf Nassef. "Design and optimization of input shapers for liquid slosh suppression". In: *Journal of Sound and Vibration* 320.1 (2009), pp. 1 –15. ISSN: 0022-460X.

[49] Brice Pridgen, Kun Bai, and William Singhose. "Shaping Container Motion for Multimode and Robust Slosh Suppression". In: *Journal of Spacecraft and Rockets* 50.2 (2013), pp. 440–448. ISSN: 0022-4650. DOI: 10.2514/1.A32137.

[50] Wisnu Aribowo, Takahito Yamashita, and Kazuhiko Terashima. "Integrated Trajectory Planning and Sloshing Suppression for Three-dimensional Motion of Liquid Container Transfer Robot Arm". In: *Journal of Robotics* (2015), pp. 1 –15.

[51] Q. Zang, J. Huang, and Z. Liang. "Slosh Suppression for Infinite Modes in a Moving Liquid Container". In: *IEEE/ASME Transactions on Mechatronics* 20.1 (2015), pp. 217–225. ISSN: 1083-4435. DOI: 10.1109/TMECH.2014.2311888.

[52] J. T. Feddema et al. "Control for slosh-free motion of an open container". In: *IEEE Control Systems* 17.1 (1997), pp. 29–36. ISSN: 1066-033X.

[53] S. J. Chen, B. Hein, and H. Worn. "Using Acceleration Compensation to Reduce Liquid Surface Oscillation During a High Speed Transfer". In: *Proceedings 2007 IEEE International Conference on Robotics and Automation*. 2007, pp. 2951–2956. DOI: 10.1109/ROBOT.2007.363920.

[54] K. Yano and K. Terashima. "Robust liquid container transfer control for complete sloshing suppression". In: *IEEE Transactions on Control Systems Technology* 9.3 (2001), pp. 483–493. ISSN: 1063-6536.

[55] K. Yano and K. Terashima. "Sloshing suppression control of liquid transfer systems considering a 3-D transfer path". In: *IEEE/ASME Transactions on Mechatronics* 10.1 (2005), pp. 8–16. ISSN: 1083-4435. DOI: 10.1109/TMECH.2004.839033.

[56] L. Consolini et al. "Minimum-time feedforward control of an open liquid container". In: *IECON 2013 - 39th Annual Conf. of the IEEE*. 2013, pp. 3592–3597. DOI: 10.1109/IECON.2013.6699706.

[57] Kazuhiko Terashima and Ken'ichi Yano. "Sloshing analysis and suppression control of tilting-type automatic pouring machine". In: *Control Engineering Practice* 9.6 (2001), pp. 607 –620. ISSN: 0967-0661.

[58] L. Moriello et al. "Control of Liquid Handling Robotic Systems: A Feed-Forward Approach to Suppress Sloshing". In: *Robotics and Automation (ICRA), 2017 IEEE International Conference on*. Singapore, 2017. DOI: 10.1109/ROBOT.2010.5509131.

[59] L. Moriello et al. "Manipulating Liquids with Robots: a Sloshing-Free Solution". Submitted to Control Engineering Practice.

[60] L. Biagiotti, C. Melchiorri, and L. Moriello. "Damped Harmonic Smoother for Trajectory Planning and Vibration Suppression". Submitted to IEEE Transactions on Control Systems Technology.

[61] Colm Ó'Dúnlaing and Chee K Yap. "A âĂIJretractionâĂİ method for planning the motion of a disc". In: *Journal of Algorithms* 6.1 (1985), pp. 104–111.

[62] Alex Yahja, Sanjiv Singh, and Anthony Stentz. "An efficient on-line path planner for outdoor mobile robots". In: *Robotics and Autonomous systems* 32.2-3 (2000), pp. 129–143.

[63] Serdar Kucuk. "Maximal dexterous trajectory generation and cubic spline optimization for fully planar parallel manipulators". In: *Computers & Electrical Engineering* 56 (2016), pp. 634–647.

[64] Jean-Claude Latombe. *Robot motion planning*. Vol. 124. Springer Science & Business Media, 2012.

[65] John Canny. *The complexity of robot motion planning*. MIT press, 1988.

[66] Jacob T Schwartz and Micha Sharir. "On the âĂIJpiano moversâĂİ problem. II. General techniques for computing topological properties of real algebraic manifolds". In: *Advances in applied Mathematics* 4.3 (1983), pp. 298–351.

[67] Bruno Siciliano et al. *Robotics: modelling, planning and control*. Springer Science & Business Media, 2010.

[68] Lydia Kavraki, Petr Svestka, and Mark H Overmars. *Probabilistic roadmaps for path planning in high-dimensional configuration spaces*. Vol. 1994. Unknown Publisher, 1994.

[69] Oussama Khatib. "Real-time obstacle avoidance for manipulators and mobile robots". In: *Autonomous robot vehicles*. Springer, 1986, pp. 396–404.

[70] Marc G Slack. "Navigation templates: mediating qualitative guidance and quantitative control in mobile robots". In: *IEEE Transactions on Systems, Man, and Cybernetics* 23.2 (1993), pp. 452–466.

[71] Ronald C Arkin. "Motor schemaâĂŤbased mobile robot navigation". In: *The International journal of robotics research* 8.4 (1989), pp. 92–112.

[72] Jerome Barraquand and Jean-Claude Latombe. "Robot motion planning: A distributed representation approach". In: *The International Journal of Robotics Research* 10.6 (1991), pp. 628–649.

[73] Chaomin Luo et al. "Sensor-based autonomous robot navigation under unknown environments with grid map representation". In: *Swarm Intelligence (SIS), 2014 IEEE Symposium on*. IEEE. 2014, pp. 1–7.

[74] Volkan Sezer and Metin Gokasan. "A novel obstacle avoidance algorithm:âĂIJFollow the Gap MethodâĂİ". In: *Robotics and Autonomous Systems* 60.9 (2012), pp. 1123–1134.

[75] Muhammad Zohaib et al. "IBA: Intelligent Bug Algorithm–A novel strategy to navigate mobile robots autonomously". In: *International Multi Topic Conference*. Springer. 2013, pp. 291–299.

[76] Luigi Biagiotti and Claudio Melchiorri. *Trajectory planning for automatic machines and robots*. Springer Science & Business Media, 2008.

[77] Luigi Biagiotti and Claudio Melchiorri. "B-spline based filters for multi-point trajectories planning". In: *Robotics and Automation (ICRA), 2010 IEEE International Conference on*. IEEE. 2010, pp. 3065–3070.

[78] Davide Chiaravalli et al. "Physical behaviour embodied in B-spline curve for robot path planning". In: *12th IFAC Symposium on Robot Control (SYROCO), 2018*. IFAC. 2018.

[79] Ildar Farkhatdinov and Jee-Hwan Ryu. "Hybrid position-position and position-speed command strategy for the bilateral teleoperation of a mobile robot". In: *Control, Automation and Systems, 2007. ICCAS'07. International Conference on*. IEEE. 2007, pp. 2442–2447.

[80] Víctor H Andaluz et al. "Switching control signal for bilateral tele-operation of a mobile manipulator". In: *Control and Automation (ICCA), 2011 9th IEEE International Conference on*. IEEE. 2011, pp. 778–783.

[81] Kiyotoshi Komuta and Toshiyuki Murakami. "An approach to expansion of workspace motion in master-slave control system". In: *IECON 2012-38th Annual Conference on IEEE Industrial Electronics Society*. IEEE. 2012, pp. 2650–2655.

[82] Cong D Pham and Pål J From. "Control allocation for mobile manipulators with on-board cameras". In: *Intelligent Robots and Systems (IROS), 2013 IEEE/RSJ International Conference on*. IEEE. 2013, pp. 5002–5008.

[83] Alberto Pepe, Davide Chiaravalli, and Claudio Melchiorri. "A hybrid teleoperation control scheme for a single-arm mobile manipulator with omnidirectional wheels". In: *Intelligent Robots and Systems (IROS), 2016 IEEE/RSJ International Conference on*. IEEE. 2016, pp. 1450–1455.